Progress in Oceanography 209 (2022) 102919

Contents lists available at ScienceDirect

Progress in Oceanography

journal homepage: www.elsevier.com/locate/pocean

A data-assimilative model reanalysis of the U.S. Mid Atlantic Bight and Gulf of Maine: Configuration and comparison to observations and global ocean models

John Wilkin [a,*], Julia Levin [a], Andrew Moore [b], Hernan Arango [a], Alexander López [a], Elias Hunter [a]

[a] Department of Marine and Coastal Sciences, Rutgers, The State University of New Jersey, New Brunswick, NJ, USA
[b] Department of Ocean Sciences, University of California, Santa Cruz, CA, USA

ARTICLE INFO

Keywords:
Coastal circulation
Numerical modeling
Data assimilation
Climatology
Sea level
Bottom temperature
Mid Atlantic Bight
Gulf of Maine

ABSTRACT

A 15-year reanalysis (2007–2021) of circulation in the coastal ocean and adjacent deep sea of the northeast U.S. continental shelf is described. The analysis uses the Regional Ocean Modeling System (ROMS) and four-dimensional variational (4D-Var) data assimilation (DA) of observations from in situ platforms, coastal radars, and satellites. The reanalysis downscales open boundary information from the Copernicus Marine Environmental Monitoring Service (CMEMS) global analysis. The dynamic model is forced by regional meteorological analyses, observed daily river discharges, and harmonic tides that augment the open boundary conditions.

A complementary analysis of the mean seasonal cycle of regional circulation, also computed using ROMS 4D-Var but with climatological mean observations and forcing, is used to reduce biases in the CMEMS boundary data and to provide a dynamically and kinematically constrained Mean Dynamic Topography to use in conjunction with the assimilation of satellite altimeter sea level anomaly observations.

The configuration of ROMS 4D-Var used is described, presenting details of the comprehensive suite of observations assembled, data pre-processing and quality control procedures, and background and observation error hypotheses. Control variables of the DA are the initial conditions, surface forcing, and boundary conditions of a sequence of non-overlapping 3-day analysis cycles.

Comparisons to a non-assimilative version of the same ROMS model configuration show the added skill brought by assimilation of local observations. The improvement that downscaling with assimilation achieves over ocean state estimates from CMEMS and the U.S. Naval Research Laboratory Global Ocean Forecast System (GOFS) is demonstrated by the reduction in residuals of the DA, and by comparison to independent (unassimilated) observations. Wherever data volumes allow, skill assessments are made with the respect to anomalies from the mean seasonal cycle to emphasize performance at the ocean mesoscale.

To highlight the utility of the analysis to inform studies related to coastal sea level variability and marine ecosystems, comparisons are made to unassimilated coastal sea level gauges and novel observations from sensors on fishing gear. The assimilation of coastal satellite altimetry data produces coastal sea level results that are coherent with observations across all time scales from interannual to tidal, while bias and correlation metrics show that bottom temperatures in regions of commercial fishing activity in the Mid-Atlantic Bight and the Gulf of Maine are modeled well.

1. Introduction

Coastal ocean circulation models that downscale global ocean simulations are valuable tools for exploring regional ocean dynamics and associated links to biogeochemistry, ecosystems, geomorphology, and other applications. The reduced geographic scope of a regional model offers computational economies that allow much greater experimentation than would be possible with global models alone, such as examining

* Corresponding author at: Department of Marine and Coastal Sciences, Rutgers, The State University of New Jersey, 71 Dudley Rd, New Brunswick, NJ 08901, USA.
E-mail address: jwilkin@rutgers.edu (J. Wilkin).

https://doi.org/10.1016/j.pocean.2022.102919
Received 15 August 2022; Received in revised form 12 October 2022; Accepted 24 October 2022
Available online 4 November 2022

sensitivity to resolution or parameterization of added physics, and they present the opportunity to affordably explore various assimilation methodologies and observation quality control strategies.

The region of interest in this modeling study is the northeastern continental shelf of North America from Cape Hatteras, North Carolina, northward to near Halifax on the Scotian Shelf of Canada, and the adjacent Atlantic Slope Sea gyre and Gulf Stream (see Fig. 1). This area encompasses several very different dynamical regimes.

In the Mid-Atlantic Bight (MAB) (Cape Hatteras to Cape Cod, Fig. 1), a permanent front at the shelf-break separates relatively fresh and cool waters on the broad (~100 km-wide) shelf from saltier, warmer Slope Sea water (Mountain, 2003). This shelf-break front is prone to instabilities with wavelengths on the order of 40 km that evolve on timescales of a few days (Fratantoni and Pickart, 2003; Gawarkiewicz et al., 2004; Linder and Gawarkiewicz, 1998), and sustain along-shelf currents that reach the seafloor driving significant flow-bathymetry interactions. A large-scale, along-shelf pressure gradient is also significant in the along-shelf momentum budget (Csanady, 1976; Lentz, 2008a; Zhang et al., 2011). Eddy shelf interactions tied to Gulf Stream-induced warm core rings (Zhang and Gawarkiewicz, 2015) also lead to cross-shelf exchange with surface and sub-surface structure at scales of 10–30 km and days to weeks. Across-shelf fluxes of heat, freshwater, nutrients, and carbon control water mass characteristics and impact ecosystem processes in the MAB.

The Gulf of Maine (GoM) is a shelf sea with local depth maxima of ~ 400 m in three distinct sub-basins. It is topographically confined and largely isolated from the Atlantic Ocean by the wide and shallow Georges Bank. Water mass characteristics in the Gulf are determined by multi-layer exchange flows through the Northeast Channel (NEC) that connects with the Northwest Atlantic Slope Sea, the shallower Northern Channel (NC) through which enters waters from the upstream Nova Scotian Shelf, and the shallow Great South Channel (GSC) to the west of Georges Bank that exchanges with the MAB (Du et al., 2021; Townsend et al., 2006; Smith et al., 2012). The region is also influenced by significant river inflows and famously strong tides that cause vigorous vertical mixing.

This spectrum of forcing mechanisms, and the dynamic shelf-edge frontal zone, make the MAB-GoM region a challenging laboratory for testing the skill of coastal ocean models and data assimilation methodologies. A great advantage to studying and modeling this region is that it is quite densely observed compared to coastal oceans globally, with much of the local data acquisition coordinated by the Mid-Atlantic Regional Association Coastal Ocean Observing System (MARACOOS) and the Northeastern Regional Association for Coastal Ocean Observing Systems (NERACOOS), both members of the U.S. Integrated Ocean Observing System (IOOS) network of coastal regional associations, which are ad hoc consortia of federal, state, academic and commercial partners. MARACOOS operations include an extensive CODAR (Coastal Ocean Dynamics Applications Radar) HF-radar network that observes surface currents from the coast to the shelf edge, and deployments of autonomous underwater glider vehicles to acquire subsurface temperature, salinity and biogeochemical data along transects throughout the MAB. NERACOOS operations emphasize a network of several telemetering buoys that observe atmospheric and ocean conditions, and prototype sustained programs observing the biogeochemical properties of the Gulf. The MAB is also home to the National Science Foundation's Ocean Observatories Initiative (OOI) Coastal Pioneer Array of seven profiling moorings and multiple deployments of autonomous vehicles, which provide very high-resolution observations in the vicinity of the MAB shelf-break front.

This paper describes the configuration, evaluation, and application of a data assimilative regional model-based circulation analysis in the MAB and GoM. The modeling system foundation is the Regional Ocean Modeling System (ROMS) (Shchepetkin and McWilliams, 2009) and its four-dimensional variational (4D-Var) data assimilation algorithms (Moore et al., 2011a; 2011b). The model design builds significantly on a prior modeling effort termed ESPreSSO (Experimental System for Predicting Shelf and Slope Optics) whose geographic scope was limited to the MAB (Zavala-Garay et al., 2014). Versions of the ESPreSSO model have been used widely for studies of hurricane-induced cooling due to ocean mixing (Seroka et al., 2017), shelf-wide ecosystems (Xu et al., 2013), carbon fluxes (Mannino et al., 2016), nitrogen cycle analysis (Hu et al., 2012), sediment transport (Dalyander et al., 2013), and as boundary conditions to yet smaller domain models (Defne and Ganju, 2015). In an assessment of 7 operational models covering the MAB region (Wilkin and Hunter, 2013), no model performed better than ESPreSSO with 4D-Var assimilation (Levin et al., 2018; Zavala-Garay et al., 2014).

In response to MARACOOS stakeholder requests for a forecast system that included not only the MAB but also the GoM, Georges Bank and the Scotian Shelf, a prototype based on the ESPreSSO design entered operations in November 2017 (Wilkin et al., 2018). Experimentation with a free-running (non-assimilative) version of the model (López et al., 2020) and with the assimilation methodology led to the multi-year 2007–2021 reanalysis to be described here. The size of the MAB and GoM model domain is double that of ESPreSSO; hence we have given this configuration the name "Doppio" (Rao, 2008).

This paper is organized as follows. Section 2 describes the Doppio modeling system, including the nonlinear forward model, the various sources of data that are assimilated, and key features of the 4D-Var configuration, including error hypotheses and observation preprocessing. In Section 3, the skill of assimilative Doppio is assessed by comparing to both assimilated and independent (not assimilated) observations. Comparisons are made with non-assimilative (NA) Doppio simulations to explore how the modeled circulation is improved by data assimilation; and with two global assimilative models, HYCOM

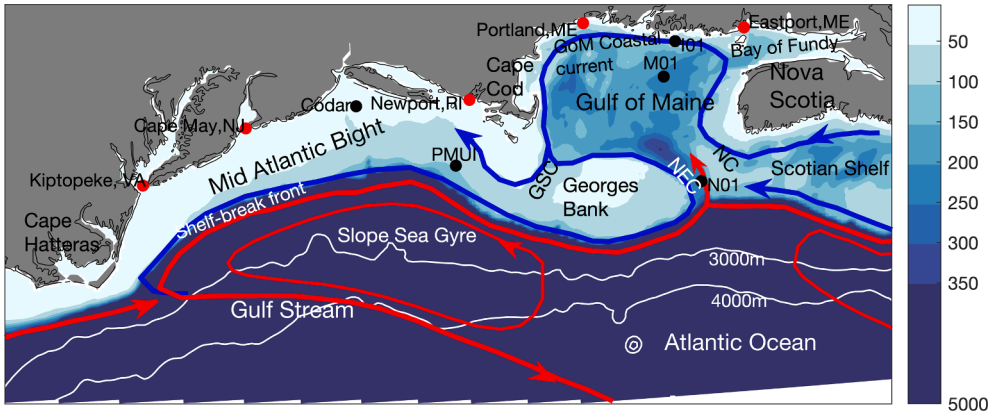

Fig. 1. Model domain, bathymetry (m, color), main currents (blue and red lines with arrows) and main geographic features. NEC – Northeast Channel, GSC – Great South Channel, NC – Northern Channel. Black dots indicate locations where surface currents comparisons are performed: NERACOOS L01, M01 and N01 buoys, Pioneer array PMUI mooring and one HF-radar location. Red dots show the locations of tide gauges. (For interpretation of the references to color in this figure legend, the reader is referred to the web version of this article.)

(Chassignet et al., 2009) and Mercator-Océan (Lellouche et al., 2018), to illustrate how a focused regional modeling effort can improve on global models of similar resolution. Both Mercator-Océan and HYCOM are elements in the international GODAE OceanView (now OceanPredict) program (Bell et al., 2015), developing and evaluating global ocean reanalysis and forecast systems. Finally, Section 3 shows that the Doppio ocean state analysis achieves skill exceeding that of the global models.

2. ROMS Doppio configuration

2.1. Nonlinear forward model setup

Doppio uses the ROMS hydrodynamic model (open-source access at https://www.myroms.org) that solves the hydrostatic, Boussinesq, primitive equations on a structured grid in terrain-following vertical coordinates. The computational kernel, described in detail by Shchepetkin and McWilliams (2009), employs a split-explicit formulation that efficiently integrates the depth-integrated momentum and continuity equations on a faster time step than the tracer and baroclinic momentum equations, with minimal aliasing of the latter. Care is taken to ensure conservation and constancy preservation of tracers when sea level displacements are a significant fraction of the water depth, as is frequently the case in coastal ocean applications. The equation of state and density Jacobian are formulated so as to minimize pressure gradient truncation errors. Collectively, these features enhance the representation of boundary layers, baroclinicity, and the vortex stretching of flow adjacent to steep bathymetry that are fundamental to steering sub-inertial frequency circulations in continental shelf seas, making ROMS an attractive choice for downscaling basin and global scale analyses to the coastal ocean.

The Doppio grid has uniform horizontal resolution of 7 km, which is adequate for the length scales that assimilation of HF-radar currents, along-track altimeter sea level and other satellite data, and relatively sparse in situ observations might reasonably be expected to constrain. The model has 40 vertical levels stretched such that in continental shelf waters the surface-most layer is 0.1 m to 1.8 m thick, and the bottom-most layer is 0.1 m to 3.4 m thick.

The model bathymetry is based on Shuttle Radar Topography Mission (SRTM) 30 arc second bathymetry data (Becker et al., 2009). To control pressure gradient errors that arise near sharp depth changes in any model with a terrain-following vertical coordinate, moderate smoothing is applied using the local smoother of Sikirić et al. (2009) to limit the roughness factor they denote as $rx_o(h)$ to be less than 0.44. Air-sea fluxes of momentum, heat, and freshwater are computed using the COARE3.0 bulk flux formulae of Fairall et al. (2003) from atmospheric fields provided by the North American Regional Reanalysis (NARR) available 3-hourly on a 33-km grid for 2007–2013 (Mesinger et al., 2006) and the North American Mesoscale (NAM) model available on a 14-km grid for 2014–2021 (Rogers et al., 2009). The vertical turbulence closure scheme is the *k-kl* parameterization implemented by Warner et al. (2005).

Daily river inflow time series were obtained by aggregating river flow gauge data from the U.S. Geological Survey (USGS) and Water Service of Canada into 27 major discharge sites, with scaling based on a statistical analysis of water balance and water transport model results (López et al., 2020) to adjust for ungauged portions of the watershed. At four major rivers in the Gulf of Maine and Bay of Fundy, the sources were split into multiple coastal cells to maintain stability during high discharge.

Information on the ocean state at the open boundaries is drawn from daily outputs of the Copernicus Marine Environmental Monitoring System (CMEMS) 1/12° horizontal resolution Mercator-Océan global data assimilation system version PSY4QV3R1 Global Ocean Physics Analysis and Forecast (Lellouche et al., 2018), hereafter referred to as *Mercator*. Mercator does not model the tides, so the TPXO global harmonic tidal analysis of Egbert and Erofeeva (2002) is used to add sea level and depth-averaged velocity tidal variability to the boundary conditions. Doppio explicitly models the ocean dynamic response to atmospheric pressure, so an inverse barometer response was added to the Mercator sea level data. The boundary data was used via a combination of active and passive perimeter radiation and nudging (Marchesiello et al., 2001) augmented by flow relaxation (Blayo and Debreu, 2006) in a nudging zone some 70 km wide around the perimeter.

Other key options and parameters of the model set-up are shown in Table 1. López et al. (2020) provide further details and assess the Doppio model skill when it runs freely without data assimilation.

2.2. Climatological mean circulation analysis

Several representations of the Doppio region mean circulation, as revealed by the sea surface mean dynamic topography (MDT), are shown in Fig. 2. When Doppio is forced at its open boundary by Mercator original fields, the Gulf Stream does not separate fully from the coast at Cape Hatteras but tends to continue along the southern MAB shelf break

Table 1
Model configuration.

Configuration	Description	Parameters
Grid resolution and time step	7-km horizontal (240 × 106 horizontal points), 40 vertical s-coordinate levels, V_{str}= 4,θ_s = 7; θ_b = 2, h_c = 250m	Baroclinic Δt = 360 s, barotropic Δt = 12 s
T,S advection scheme	NL model: 4th order Akima horizontal and vertical, TL/AD models: 3rd order upstream biased horizontal, 2nd order centered vertical	
Velocity advection	3rd order upstream biased horizontal, 4th order centered vertical	
Horizontal mixing	2nd order harmonic T,S mixing along z-levels, velocity mixing along s-levels	Diffusivity 50 $m^2\ s^{-1}$, viscosity 100 $m^2\ s^{-1}$
Vertical turbulence closure	GLS k-kl, Craig-Banner wave breaking, Kantha-Clayson stability function, horizontal smoothing of buoyancy and shear, splines reconstruction of vertical shear	
Pressure gradient	Splines density Jacobian, imposed atmospheric pressure	
2-D lateral open boundary conditions	Implicit Chapman for SSH; Flather for $\bar{u}$,$\bar{v}$ with harmonic tide (MS4, M4, MN4, K2, S2, M2, N2, K1, P1, O1, Q1) from TPXO added to bias corrected Mercator fields.	
3-D lateral open boundary conditions	NL model: Radiation with nudging to bias corrected Mercator solution; TL/AD models: clamped	Nudging 0- to 10-day timescale in 70-km zone for T,S
Surface heat and momentum fluxes	Fairall (2003) bulk flux formula, wind minus current in stress, downward longwave radiation from NARR and NAM, outgoing longwave from model SST; local diurnal cycle modulates daily average shortwave radiation	Jerlov water type 4 for vertical penetration of solar radiation
Bottom drag	Quadratic bottom drag	C_D = 0.003
River sources	Gauge data from USGS and Water Survey of Canada, 27 major rivers; St. John, Penobscot, Kennebec, Merrimac rivers split into branches	Volume influx point sources LwSrc = T
Assimilation	RBL4DVAR adjusting initial and boundary conditions, wind stress and heat flux; iterations use 2 outer and 7 inner loops over 3-day assimilation window	Horiz. de-correlation scales: 40 km for SSH/U/V/T, 15 km for S, vertical 10 m.

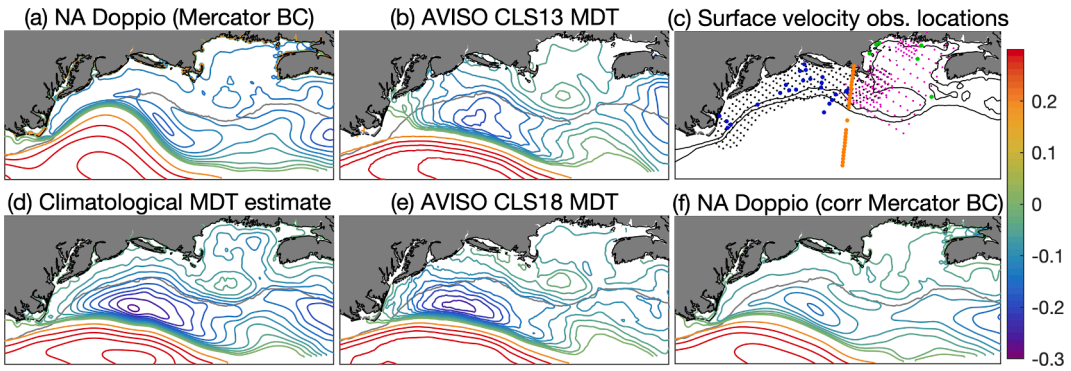

Fig. 2. (a) Mean 2007–2021 Sea Surface Height (SSH) from NA Doppio forced by Mercator at the boundary; (b) AVISO CNES CLS13 MDT; (c) locations of velocity observations from HF-radar (black dots), GoM drifters (magenta dots), moored current meters (blue dots), NERACOOS moorings (green dots) and from Line-W moorings (orange dots); (d) Mean SSH climatological estimate; (e) AVISO CNES CLS18 MDT; (f) NA Doppio forced by bias-corrected Mercator at the boundary. A grey line on the contour plots indicates the 500-m isobath used as a threshold criterion for altimetry assimilation. Black lines in (c) correspond to 50 m and 100 m isobaths. (For interpretation of the references to color in this figure legend, the reader is referred to the web version of this article.)

upsetting the strength of the Slope Sea gyre and suppressing southwestward flow that should be present along the continental slope (contrast Fig. 2a and 2c). We are unsure of the precise cause of this problem, but the issue is largely eliminated when we adjust for biases in the Mercator boundary data using a dynamically constrained 3-D regional climatological analysis. The climatological analysis, described in this section, also provides a consistent MDT to use in altimeter sea level data assimilation.

The annual and monthly mean climatological analysis was produced following an approach similar to that of Levin et al. (2018) for ESPreSSO, wherein the Doppio model is driven with climatological mean external forcings (fluxes, stresses, rivers, and boundary conditions) constrained by data assimilation of long-term historical observations. The ROMS model equations impose additional dynamical and kinematic (regional bathymetry and coastline) constraints on the resulting climatological solution.

The mean observations assimilated are detailed in Table 2. They include our own gridded Mid-Atlantic Ocean Climatological Hydrographic Analysis (MOCHA) (Fleming 2016; Wilkin and Fleming, 2017) of historical temperature and salinity observations, and mean velocity estimates from several years of HF-radar currents, long-duration moored current meter deployments, and drifters (Fig. 2c). In addition, where the ocean depth is greater than 500 m, the AVISO CNES-CLS13 MDT (Rio et al., 2014) (the version available at the time of the analysis) (Fig. 2b) was treated as sea level data for assimilation so as to enforce consistency between our regional coastal MDT and that of AVISO in the open ocean. MDT contours align strongly with streamlines of the depth-integrated flow; using AVISO MDT information only seaward of 500 m (which is little different from 1000 m or even 2000 m) is our heuristic approach to rejecting features in the coastal ocean (Fig. 2b) that appear qualitatively implausible to us, such as MDT contours that dramatically intersect isobaths in most of the shelf seas.

The first step in the climatological analysis was to compute an annual mean Doppio solution using MOCHA (Fleming 2016) hydrography and annual mean sea surface height (SSH) and velocity from Mercator for initial and boundary conditions, forced by annual mean river inflows and air-sea fluxes. Next, the observation-based estimates of mean conditions were assimilated using 4D-Var with a 2-day analysis window during which the observations were repeated frequently to penalize time evolution of the solution: temperature and salinity are repeated every 4 h; velocity and SSH are repeated every 30 min (see Levin et al. 2018 for full details). Finally, the average of the converged model solution over the assimilation window becomes the completed analysis.

The resulting mean SSH (Fig. 2d) is close to both AVISO CLS13 and the newer AVISO CLS18 MDT (Mulet et al., 2021) (Fig. 2e) in the open ocean. There is a steady southwestward flow along the MAB shelf, recirculation around Georges Bank, and a system of coastal currents in the GoM in good agreement with estimates from Lentz (2008a), Lentz (2008b) and Feng et al. (2018). Comparison of the two versions of AVISO MDT (Fig. 2b,e) indicates the progress that AVISO has made towards improving the representation of coastal circulation. However, in comparison to Fig. 2d, CLS18 still exhibits many MDT contours dramatically intersecting the coast, an unrealistic reversal in the alongshelf sea level slope at the coast in the southern the MAB, a weak GoM coastal current system, the absence of closed MDT contours indicating topographically driven re-circulation around the deep basin in the GoM, and weak horizontal exchange flow through the Northeast Channel.

The second step in this procedure was to compute a set of 12 analyses, one for each month, to estimate the seasonal cycle of SSH and velocity that is dynamically consistent with MOCHA. The initial and boundary conditions were from MOCHA monthly hydrography and monthly mean Mercator SSH and velocity that was bias corrected by

Table 2
Observations used in ROMS Doppio climatological analysis.

Observation type and platform	Source	Time coverage space/time resolution
MOCHA climatology	Wilkin and Fleming (2017)	40 years, monthly, 5 km, 57 standard depths
Velocity from current meters in MAB and Slope Sea	Lentz (2008a,b)	35 years, 25 profiles
AVISO MDT	AVISO.altimetry.fr auxiliary products CNES-CLS13 (Rio 2014)	1993–2012 mean of altimeter passes, fields at 1/8° grid
Surface currents from CODAR HF-radar	maracoos.org/index.php/download	2006–2021, 1-hour, 6-km
Velocity from Line-W ADCP	Toole et al. (2011)	4 moorings during 2001–2009
Velocity from NERACOOS moorings	https://www.neracoos.org/erddap/search/index.html?searchFor=historic+currents	6 moorings during 2001–2010
Velocity from GoM drifters	Manning et al. (2009)	227 drifters, 1988–2007 analyzed into 50 km Eulerian field

replacing the Mercator annual mean with the annual climatological analysis described above, with external forcing being the appropriate climatological monthly-mean river inflows and air-sea fluxes. The analysis assimilated monthly MOCHA climatology and monthly mean observations of velocity. There is no monthly AVISO MDT to utilize, so to constrain velocity in the Slope Sea and Gulf Stream we assimilate geostrophic velocities below 100 m that were calculated from monthly MOCHA hydrography referenced to 2000 m.

The assimilation procedure drives the model toward a quasi-steady climatological mean solution with 4D-Var adjusting the 3-dimensional ocean state, boundary conditions, and air-sea fluxes to minimize the model-observations misfit. The approach effectively treats MDT and the seasonal cycle of velocity and SSH as diagnostic quantities that arise when a high-resolution circulation model enforces dynamical consistency and the influence of coastline and bathymetry on the flow field, while data assimilation further constrains the 3-D flow to match what is known from long-term observations.

The monthly climatological analysis is used in the bias correction of Mercator fields, and the annual mean climatological analysis provides the mean dynamic topography (MDT) that is added to altimetry sea level anomaly to produce observations of total SSH suitable for assimilation (further details in Section 2.6).

2.3. Bias correction of boundary conditions

One of the advantages of the Mercator PSY4QV3R1 reanalysis, introduced in 2016, is that it was released with a consistent reanalysis of the prior decade. This allows us to reliably estimate the 2007–2021 mean seasonal cycle of temperature and salinity and replace it with our seasonal climatological analysis. Fig. 3 illustrates the character of the adjustment by showing the annual mean of temperature and salinity bias correction for the three Doppio open boundaries. Latitude is shown on the x-axis, and vertical black lines separate the three boundaries: Cape Hatteras across the Gulf Stream to the Atlantic Ocean (left), Atlantic Ocean (middle), and Atlantic to Scotian Shelf (right). The adjustment reduces the depth of the incoming Gulf Stream, and its extent along the open ocean boundary.

Seasonal bias corrections to temperature and salinity were applied based on harmonic analysis of 2007–2018 daily Mercator fields and monthly climatology. This introduced a smooth adjustment in the deep ocean and seasonal thermocline, but it proved necessary to relax back to the original Mercator values in the mixed layer. Annual mean and seasonal Mercator SSH and velocity were similarly replaced with values derived from the Doppio monthly climatological 4D-Var analyses described in Section 2.2.

Removing bias from the Mercator boundary conditions was crucial in overcoming the problems with Gulf Stream separation. When free-running Doppio (no assimilation) is forced by bias-corrected Mercator at the boundaries, the mean SSH (Fig. 2f) demonstrates better agreement with our climatological analysis (Fig. 2d). By design, the bias correction procedure affects only the long-term mean flow; mesoscale and inter-annual variability in the Mercator boundary conditions data is retained.

2.4. 4D-Var algorithm

ROMS supports a suite of several implementations of 4-dimensional variational (4D-Var) data assimilation that are complemented by post-processing and analysis tools for a variety of applications. The system is described in detail by Moore et al. (2011a, 2011b, 2011c). In addition to our own work in the MAB (Levin et al. 2020, 2021a, 2021b), ROMS 4D-Var has been applied to studies of circulation in the California Current system (Neveu et al., 2016), Intra-Americas Sea (Powell et al., 2008), East Australian Current (Kerry et al., 2016), Yellow Sea (Lee et al., 2018), Adriatic Sea (Janeković et al., 2020) and elsewhere.

The assimilation algorithm used in Doppio is the incremental, strong constraint, dual formulation of 4D-Var using the Restricted B-preconditioned Lanczos (RBL4DVAR) formulation of the conjugate gradient method in which the cost function (comprising contributions from the model-data misfit and the perturbation from the background, or prior, estimate) is minimized directly in the space spanned by the observations (Gürol et al., 2014).

For a chosen analysis interval, the system produces optimal initial conditions, and optimized boundary conditions, wind stress and surface heat flux. Subject to these initial and boundary conditions, the nonlinear model simulation over the analysis interval becomes the “best” analysis of the model state. An assimilation window of three days was determined to be sufficiently small to ensure that the linearization assumption of the incremental method is valid (Zhang et al. 2009). The solution at the end of each 3-day analysis interval becomes the initial conditions to the prior state vector, or “background”, for the next assimilation cycle. These successive 3-day cycles are concatenated to form the 15-year analysis. Two outer and seven inner loops are used in the iterative algorithm. Our experience with Doppio is that further iterations typically accomplish little in reducing the cost function. More detail on the Doppio 4D-Var model setup can be found in Wilkin et al. (2018).

2.5. Background model error hypothesis

The background model error hypothesis is crucial to achieving successful 4D-Var assimilation. ROMS specifies these errors as a univariate correlation matrix scaled by the square of standard deviations provided by the user. The background error standard deviations used for Doppio were computed from daily average fields from a 2007–2020 non-assimilative Doppio simulation after first removing a least-squares fit to the mean seasonal cycle; this ensures the standard deviations represent mesoscale variability. Monthly ensemble estimates of background standard deviations are harmonically interpolated to daily values to provide a smooth transition through seasonally changing mesoscale

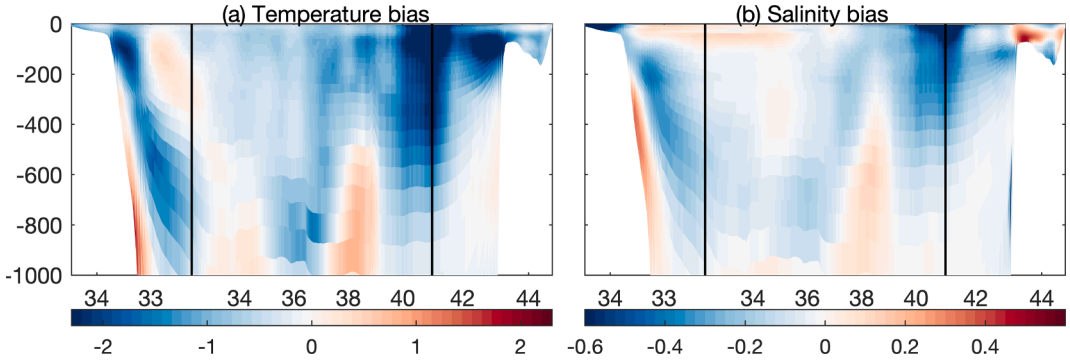

Fig. 3. Mercator annual mean bias correction in temperature and salinity (climatology minus Mercator) along Doppio boundaries (southwest – open ocean – northeast); x-axis shows latitude along the boundaries.

variability.

As described in Moore et al. (2011c), the 4D-Var background error covariance matrix was modeled following the diffusion operator approach of Weaver and Courtier (2001). In principle, the horizontal and vertical decorrelation scales should vary within the domain depending on differences in the circulation, and through time to reflect seasonal changes. Currently, the ROMS 4D-Var formulation does not allow spatially variable decorrelation scales, so constant values were used throughout: a horizontal scale of 40 km was chosen for temperature, SSH and velocity, and 15 km for salinity. These scales were estimated using a binned-lagged covariance analysis of output from the same 2007–2020 free run used to compute the background error standard deviations. A scale of 100 km was used for wind stress and heat flux.

During winter, larger vertical decorrelation scales help propagate information about the mesoscale from surface observations down through the water column, but an overestimation of the vertical decorrelation scale in areas characterized by strong summer stratification can drive spurious vertical oscillations. We found it impractical to provide a smooth transition of the decorrelation scales through the abrupt seasonal breakdown of stratification so we kept decorrelation scales constant through time based on the shortest vertical decorrelation scale, 10 m, estimated over the whole domain. While this may limit the influence of surface observations in the open ocean, the integrity of the summertime circulation in the MAB and GoM is preserved.

2.6. Sources, processing and quality control of observations

We have gone to extensive lengths to assemble, for data assimilation, the most comprehensive set possible of all regional observations of ROMS state variables – temperature, salinity, velocity and sea level – from both in situ and remotely sensed sources.

It has been shown recently (summarized by Cipollini et al., 2017) that satellite altimeters offer a wealth of valuable sea level observations in coastal waters. Accordingly, we utilize altimeter along-track sea surface height anomaly (SSHA) data from Jason 1, 2 and 3, EnviSat, AltiKa, CryoSat, and Sentinel-3 accessed via the Radar Altimeter Database System (RADS) with range and geophysical corrections that retain coverage close to the coast (Feng and Vandemark, 2011). Satellite Sea Surface Temperature (SST) data from complementary infrared and microwave sensors were collected; namely, AVHRR, VIIRS, AMSRE, AMSR2, TRMM, WinSAT, and GOES satellites. Ocean surface current data from the MARACOOS coastal HF-radar network were assimilated as 6-km resolution, 1-hour interval vector velocities gridded and combined by optimal interpolation (Roarty et al., 2010).

Numerous in situ temperature and salinity data sets were assimilated. In the GoM, 10 NERACOOS moorings that each host several fixed depth CTD sensors provide hourly measurements, with occasional gaps, for most of 2007–2021. In the MAB, MARACOOS operates Autonomous Underwater Glider Vehicles from the coast to the continental shelf-break. Further in situ observations (from gliders, Argo profiling floats, XBTs, NDBC moored and drifting buoys, and vessel underway thermosalinograph) were obtained from the EN4 quality-controlled database provided by the United Kingdom Met Office (UKMO) (Good et al., 2013) and from National Marine Fisheries Ecosystem Monitoring (ECOMON) voyages (McClatchie et al., 2014).

Contrasting the distribution of data accessible to us with the comparable data set assimilated in Mercator-Océan, Wilkin et al (2018) showed that our data assembly activity has very effectively harvested a wealth of local information with the potential to significantly improve state estimation by data assimilation, especially in coastal areas.

Where observation sampling is more dense in space and/or time than the model resolution and time step (especially observations from gliders, and the vertical sampling of Argo floats), or where observations are noisy (e.g., HF-radar velocities), then observations are combined to form so-called super-observations, a standard practice in data assimilation (Daley 1991). Super-observations are data averages, weighted by inverse observation error variance, within chosen space and time bins. The formation of super-observations reduces data redundancy and poor conditioning of the cost function with respect to minimization.

The number of satellite SST observations is very large, and their spatial resolution is mixed. Depending on sensor resolution, satellite SST observations were first either binned (polar orbiter infrared) or interpolated (microwave) to grid cells, while due to their noise, geostationary infrared SST observations were first averaged in 24 km bins before interpolating to grid cells. Then, aggregating the data in 6-hourly intervals to compute super-observations, microwave and geostationary observations were used only in those grid cells that did not have polar orbiter infrared measurements. In situ temperature and salinity profiles were also binned in the vertical on the same standard depth levels as the World Ocean Database (Boyer et al., 2009). Altimeter SSHA observations were averaged if the tracks intersected within 7 km in a 2-hour interval.

The pre-processing of altimeter SSHA requires some detailed explanation. In conventional applications of altimetry, high-frequency signals are removed by applying tide, inverse barometer (IB), and Dynamic Atmosphere (DAC) corrections. But here, all these dynamics are present in the model, so none of these high-frequency corrections were applied.

However, out of concern that even small phase errors in the tide stemming from Doppio's relatively low resolution (for a tidal model) might dominate model-data misfit for SSH, we modified the tide signal in the altimeter observations. The data were first de-tided using the GOT4.10 (Ray, 2013) harmonic tide, and then a new tide signal was added using the harmonic tide computed from NA Doppio. In this way the misfit between modeled and observed SSHA should be dominated by the non-tidal dynamics that we seek to constrain by assimilation. To the SSH anomaly from altimetry we add the MDT computed from the climatological analysis of section 2.2 so that the observations and bias corrected Mercator boundary conditions are consistent. The accurate coastal MDT also means that altimeter data can be used to within tens of kilometers from the coast. Finally, so that sea level outputs are useful as boundary conditions for higher resolution estuarine models or studies of coastal inundation, we impose a constant offset to SSH (López et al. 2020) to bring the model sea level datum as close as possible to the North American Vertical Datum of 1988 (NAVD88).

Proximity analysis was performed for all observations to remove outliers. In situ temperature and salinity were flagged as outliers if they were more than five background model standard deviations from MOCHA climatology. Satellite SST observations were similarly quality controlled based on statistics derived from a multi-platform optimum interpolated SST data set (Remote Sensing Systems, 2017).

Further quality control was performed during the 4D-Var analysis itself using the ROMS Background error Quality Control (BGQC) strategy in which observations that deviate too far from the expected total error were rejected based on a chosen threshold. The thresholds applied for sea level, velocity, temperature and salinity were 2.2, 2.5, 2.8 and 2.8 standard deviations, respectively, which eliminate a modest subset of observations (not more than 5 %).

On a typical day the system assimilates some 250 T,S observations from moorings, 200 T,S observations from gliders and Argo floats, 100 in situ T,S values from other platforms, 300 SSHA altimeter observations, 5000 HF-radar current vectors, and 50,000 SST observations, counting binned quality-controlled observations only. More detail on observations, their sources, and binning strategies are provided in Table 3 and Wilkin et al. (2018).

2.7. Observation error hypothesis and its relationship with background errors

Another important component in successful 4D-Var assimilation is an appropriate observation error hypothesis that takes into account both sensor and representation error. For some platforms (e.g., infrared SST),

Table 3
Observations, and their corresponding assumed error, that were assimilated into ROMS Doppio reanalysis. For some data types, the observation error may be scaled by the background error standard deviation, σ_{bg}, and the standard deviation of observations binned in the vertical, σ_{vb}.

Observation type and platform	Source	Sampling frequency and resolution	Super-observation space/time averaging	Observation error: Absolute or scaled by standard deviations
Infrared SST: AVHRR, VIIRS	MARACOOS maracoos.org	4 passes per day, 1 km	6-hour; grid resolution bins	0.6 °C
Infrared SST: GOES	NOAA CoastWatch coastwatch.pfeg.noaa.gov	Hourly, 6 km	6-hour; grid resolution, interpolated from 24 km bins	1.4 °C
Microwave SST: AMSRE, AMSR2, TRMM and WindSat	NASA PODAAC podaac.jpl.nasa.gov	1 to 2 passes per day, 15 km	At obs. time; grid resolution interpolated	0.7 °C
SSHA: Satellite altimeters Jason-1,2,3, EnviSat, AltiKa, CryoSat, Sentinel-3 with coastal corrections	RADS rads.tudelft.nl	Usually 1 pass per day in domain, 7 km along-track	Repeated every 6 min over 3-hour period (see section 2.7); grid resolution	4 cm
In situ T,S: NDBC buoys, Argo floats, shipboard XBT, surface drifters	UKMO En4.2, ECOMON	Varies with platform	Binned to vertical standard depths; repeated every 2 h over 2-day period (section 2.7)	$\max(0.1, s)$ where $s = \sigma_{bg}\max(0.33, \frac{\sigma_{vb}}{\max\sigma_{vb}})$
Surface currents: CODAR HF-radar	MARACOOS maracoos.org	Hourly, 6 km	1 h; 24 km	$\max(7\text{cm s}^{-1}, 0.5\sigma_{bg})$
In situ T,S: Gliders ~ 1–2 deployments per month in domain by MARACOOS	NOAA IOOS Glider DAC gliders.ioos.us	Dense along trajectory	Binned to vertical standard depths and 2-hour along track	$0.6\max(0.1, s)$ where $s = \sigma_{bg}\max(0.33, \frac{\sigma_{vb}}{\max\sigma_{vb}})$
In situ T,S: Gulf of Maine buoys	NERACOOS neracoos.org	Hourly, 10 buoys	1 h, no binning in the vertical	0.9 σ_{bg} for T, 0.6 σ_{bg} for S
In situ currents: ADCP on Gulf of Maine buoys	NERACOOS nearcoos.org	Hourly, 9 buoys	1 h, binning in the vertical	$\max(2\,\text{cm s}^{-1}, 0.5\sigma_b)$

observation sensor error is well established and quite consistent, while for others, such as HF-radar combined vector currents, it varies within the dataset in ways that are difficult to characterize. Representation error stems partly from dynamics that are not modeled or resolved but may be present in the observations, such as nonlinear internal waves, submesoscale turbulence, or a particularly sharp thermocline. The ratio between background error and observation error is important because it determines how much trust the system puts in observations compared to the model. If the observation error is too large compared to the background the analysis will ignore the observation. If the observation error is too small, the analysis may develop an unphysical response to assimilation due to over-fitting (e.g., fast barotropic waves that travel around the coastline over several hours after reinitialization, or buoyant eddies that appear around an in situ point observation if it differs from the model estimates too much). Duplicating observations at short lags using inflated observation errors, rather than assimilating a single observation with small observational error, reduces these artifacts. To ensure we have achieved a valid balance between background and observational error hypotheses an a posteriori analysis following Desroziers et al. (2005) was also performed.

Starting from various a priori observation error hypotheses based on instrument accuracy and previous experience (for representation error), and background error hypotheses related to mesoscale variability of the free model run (Section 2.5), we conducted a series of short (weeks to months) assimilation experiments to inform a posteriori analyses of the covariances of observation, background and estimation errors in observation-space to guide adjustments to the prior assumptions. Desroziers et al. (2005) (see also Mattern et al., 2018) postulate that for self-consistent error statistics both $\widetilde{\sigma}_o/\sigma_{obs}$ and $\widetilde{\sigma}_b/\sigma_{bg}$ should be close to one, where σ_{obs} and σ_{bg} are mean observation and background standard deviations respectively, and the Desroziers' residual and innovation statistics are the covariances

$$\widetilde{\sigma}_o = \sqrt{\left(\varepsilon_{po}{}^T \varepsilon_{pr}\right)/N} \text{ and } \widetilde{\sigma}_b = \sqrt{\left(\varepsilon_{inc}{}^T \varepsilon_{pr}\right)/N}$$

calculated from $\varepsilon_{po} = y - x^a$, which is the vector of assimilation residuals (difference between observations and posterior estimate), $\varepsilon_{pr} = y - x^b$, which is the vector of innovations (difference between observations and prior estimate) and $\varepsilon_{inc} = x^a - x^b$, which is the vector of increments (the change made by assimilation); N is the number of observations.

For temperature and salinity, the Desroziers' statistics analysis led us to reduce our initial estimate of background error standard deviation in the mixed layer, and to rescale the in situ observation error with the background error to make model-data misfit reduction more uniform across different dynamic regimes. The scaling factors were adjusted separately for each observational platform and are detailed in Table 3.

The ROMS 4D-Var formulation assumes that observation errors are uncorrelated in space and time. For sparse or occasional observations, like ship-based measurements and along-track altimetry, 4D-Var may generate short wavelength oscillations if they are assimilated with too small observational error. For observations that are dense or frequent (buoy- and glider-based observations, HF-radar) the response is typically more smooth. To obtain a smoother response to point observations, they were assimilated repeatedly over a specified time window using larger observation errors, effectively propagating their information in time. Ideally, this would be achieved with a time correlation in the 4D-Var observation operator, but that is a feature not presently available in ROMS RBL4DVAR. The repeat window, frequency of repeats and corresponding observation errors were adjusted with guidance from the Desroziers analysis: the ship-based temperature and salinity error statistics are closest to optimal if these observations are repeated every 2 h within a two-day time interval (at actual time ±1 day). Similarly, it was determined that each altimeter pass is better assimilated on every time step (every 6 min) within a 3-hour time interval, principally to suppress the generation of spurious gravity waves. The eventual choice of observation errors is shown in Table 3, where some observation errors are absolute, and others are scaled according to the background variance mostly in recognition of representation error.

The mean ratios $\widetilde{\sigma}_o/\sigma_{obs}$ and $\widetilde{\sigma}_b/\sigma_{bg}$ (when the error hypotheses in Table 3 are used) are shown in Table 4. They are acceptably close to 1, with observation error slightly less than optimal and model error slightly greater than optimal. The ratios of mean residual to mean innovation, $\varepsilon_{po}/\varepsilon_{pr}$, (bottom row of Table 4) indicate that assimilation reduces model-data misfit for all observation types, with the largest reduction for SSH followed by in situ T,S. Error reduction for SST is modest, but this is

Table 4
Desroziers statistics. σ_{bg} is background error standard deviation, σ_{obs} is observation error standard deviation, $\widetilde{\sigma}_o$ and $\widetilde{\sigma}_b$ are Desroziers' residual and innovation statistics, respectively, and ε_{po} and ε_{pr} are RMS of residuals and innovations, respectively.

	SSH	u-velocity	v-velocity	SST	in situ T	in situ S
$\widetilde{\sigma}_o/\sigma_{obs}$	1.31	1.34	1.11	1.03	1.31	1.16
$\widetilde{\sigma}_b/\sigma_{bg}$	0.75	0.71	0.91	0.81	0.71	0.71
$\varepsilon_{po}/\varepsilon_{pr}$	0.29	0.79	0.86	0.77	0.66	0.62

expected given it is strongly controlled by 2-m air temperature from the meteorological forcing; generally speaking, SST is not a challenging test of ocean model skill. As noted by Levin et al. (2021), velocity observations have limited impact on the predominantly geostrophically balanced circulation at 7-km resolution, but would emerge as more impactful when resolution increases and admits more unbalanced dynamics.

3. Skill assessment and intercomparison of models

The Mercator-Océan system of CMEMS and the HYCOM model (Chassignet et al., 2009) operated by the U.S. Naval Research Laboratory (NRL) are two global models of ~ 1/12° resolution that are widely used both to study regional oceanic processes, and to provide boundary conditions for regional ocean models. Given that the global analyses are data assimilating and have resolution only marginally coarser than Doppio, a reasonable question to ask is whether regional down-scaling with assimilation adds value to those global models?

This section uses various metrics to contrast the skill of Doppio analysis with the global analyses. The same metrics are also used to compare the Doppio assimilative analysis with a free-running non-assimilative (NA) Doppio (Wilkin et al., 2018; López et al., 2020) to explicitly examine the value added by regional data assimilation.

Mercator results are version PSY4QV3R1 daily outputs (Lellouche et al., 2019). The NRL HYCOM group do not recompute historic fields when introducing new versions, so we merge daily fields for 2007–2018 from the Global Ocean Forecasting System (GOFS) 3.0 GLBu0.08/expt_19.1 to expt_91.2 with 3-hourly fields for 2018–2021 from GOFS 3.1 GLBy0.08/expt_93.0 (Metzger et al., 2017). So that it is clear that we are using results from the HYCOM modeling system with data assimilation as implemented at NRL, hereafter we refer to these results as simply GOFS.

Skill is appraised by comparing model results with available observations, both assimilated and independent (not assimilated). Details of the independent observations are given in Table 5. All the comparisons are performed using daily averaged model output fields unless otherwise stated.

3.1. Mean circulation and variability in sea level and surface currents

Assimilation of the full suite of time-varying observations yields a mean SSH from Doppio 2007–2021 reanalysis (Fig. 4a) that is closer to the climatological SSH (Fig. 2d) than SSH from NA Doppio (Fig. 4d). Improvements include strengthening of the Shelf Slope front, Slope Sea gyre, circulation around Georges Bank, and the flow in and out of GoM through the Northeast Channel. Compared with NA Doppio, assimilative Doppio reanalysis demonstrates a stronger GoM coastal current and southwestward MAB shelf circulation. However, these are somewhat weaker than in our climatological mean estimate (Fig. 2d) that is obtained by heavily penalizing deviations of the model from climatological observations (Section 2.2). We attribute the skillful representation of mean coastal sea level features to the assimilation of altimeter data across the continental shelf with an accurate MDT. Mercator and GOFS (Fig. 4b,c), which also assimilate SSH, show a mean bias (model SSH minus climatological SSH) in the form of a weaker Gulf Stream and Slope Sea gyre, and substantially weaker and less well-organized coastal currents.

To examine model skill in capturing mesoscale variability, correlations with Jason 1–3 along-track sea level anomalies (third row of Fig. 4) were computed after first removing a harmonic fit to the mean seasonal cycle (which would otherwise dominate the variance, and give an inflated sense of skill). In the case of Doppio, these anomalies from the mean seasonal cycle were filtered with a 3-day running average to remove time scales that are not present in the global models. Similar relative performance of the models is evident in RMSE (bottom row of Fig. 4). For Doppio, RMSE is greatest proximate to the domain perimeter where the Gulf Stream exits, perhaps indicating an imperfect open boundary condition, yet it is less than for the global models that have no boundary in that location.

Correlations are low for NA Doppio because it does not capture event-wise correspondence in mesoscale processes. Assimilative Doppio, on the other hand, is best in capturing mesoscale variability across the whole domain. Its superiority is especially pronounced in coastal areas due, presumably, to the assimilation of coastal ocean altimetry data up to the 10-m isobath in the MAB and GoM; neither Mercator nor GOFS utilize coastal altimetry data.

The ability of Doppio to capture sea level variability at the coast is further evident in Fig. 5, which shows the coherence of model SSH with independent hourly sea level measurements from five representative NOAA coastal tide gauges distributed throughout the MAB and GoM (sites shown in Fig. 1). The spectra are computed by standard periodogram smoothing (Moore and Wilkin, 1998); degrees of freedom are difficult to estimate so the time series are deemed incoherent and squared coherence is not plotted when it is less than 0.1.

The Doppio reanalysis performs very well by consistently capturing coastal sea-level variability better than any other model on all time scales. Aside from data assimilation, the two Doppio models are otherwise identical and we presume it is the altimeter data that improves coherence with the tide gauge data from mesoscale to seasonal and multiyear scales. Mercator and Doppio have similar coherence with observations on seasonal to multiyear scales, but Mercator is considerably less coherent than Doppio in the mesoscale. We attribute this to the assimilation of coastal altimetry being absent in Mercator. GOFS has similar skill as Mercator in the mesoscale, but is poor at capturing multiyear variability.

Daily data were used for Mercator and GOFS, so the spectra end at the Nyquist frequency of 0.5 day^{-1}, while for hourly Doppio output the comparison extends to 1 day^{-1}. By design, both Doppio versions share

Table 5
Independent (non-assimilated) observations used in model validation.

Observation type and platform	Source	Time coverage space/time resolution	Geographic Area
Sea level from tide gauges	NOAA CO-OPS opendap.co-ops.nos.noaa.gov	2007–2021, hourly	MAB and GoM near coast
Near surface velocity from moored ADCP	NSF OOI Pioneer Array ooinet.oceanobservatories.org	2013–2019, 15 min	MAB shelf break
Aanderaa surface currents	NERACOOS neracoos.org	2007–2021, hourly	GoM
Temperature and salinity CTD profiles	NSF OOI Pioneer Array ooinet.oceanobservatories.org	2013–2020, hourly	MAB shelf break
Bottom temperature	NOAA NEFSC fishing Study Fleet (Manning and Pelletier, 2020); commercial lobster traps (Manning and Pelletier, 2014)	2015–2021, various depths	MAB and GoM
Surface salinity from satellite	SMAP v4 (Meissner et al., 2019)	2015–2021, monthly	Whole domain
Surface salinity from thermosalinograph on research vessels	NOAA AOML https://www.aoml.noaa.gov, and NCEI ncei.noaa.gov (Wang, 2017)	2009–2021, various	MAB and GoM

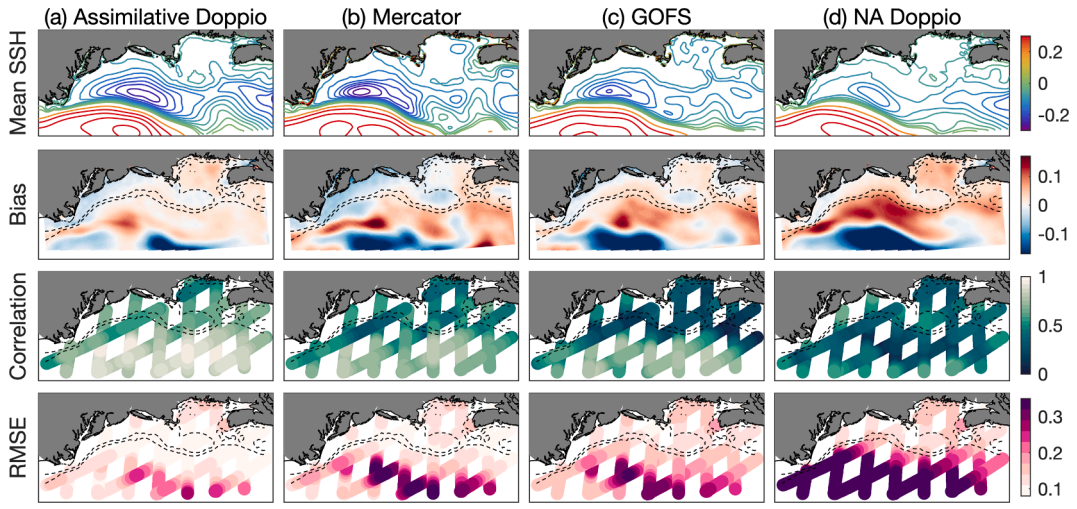

Fig. 4. Mean SSH (m) (top row), bias (mean SSH minus climatological MDT) (second row) and correlation (bottom row) between SSH anomaly from Jason 1–3 missions and SSH anomaly for (a) Doppio, (b) Mercator, (c) GOFS and (d) NA Doppio models for 2007–2021 time period.

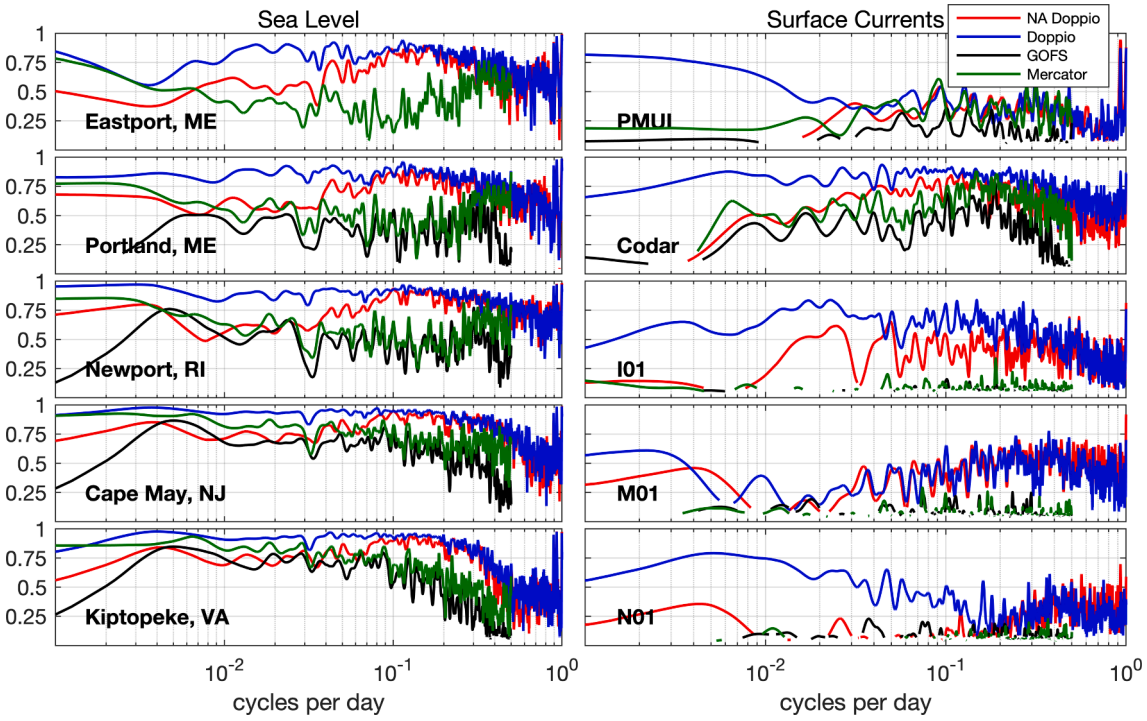

Fig. 5. Squared coherence in 2007–2021 between the models and (left column) sea level from five coastal tide gauges, and (right column) near-surface currents from CODAR, NERACOOS, and Pioneer array. See Fig. 1 for observation locations. Models are Doppio (blue), NA Doppio (red), Mercator (green), and GOFS (black). The Eastport, ME, tide gauge is too far removed from a valid "water" point in the GOFS land-sea mask and is not plotted. Velocity directions are aligned with the axis of the NEC at N01, and along-coast at other moorings. A vertical average of velocity in the upper 20 m is used at PMUI; surface velocity is used at other locations. (For interpretation of the references to color in this figure legend, the reader is referred to the web version of this article.)

the same boundary tidal harmonic forcing with steps taken (Section 2.6) not to upset the tidal response through assimilation. At these highest frequencies, the Doppio models are significantly coherent with observations due to the ROMS model dynamics responding faithfully to sufficiently accurate tides and high frequency local meteorological forcing.

Coherence between modeled and observed near-surface velocity is shown in the righthand column of Fig. 5. At Pioneer Array site PMUI (Upstream Inshore Profiler Mooring) a depth average of the upper 20 m of ADCP data is used to assess the skill of the models near the MAB shelf break. None of the models assimilated these data, yet all four are coherent with observations at short time scales (though less so for GOFS). However, the skill at mesoscales and seasonal scales is vastly different. The assimilation of altimetry and HF-radar dramatically improves Doppio coherence at the longer time scales; NA Doppio is incoherent with PMUI observations at those scales. The two global models are less coherent with observations than Doppio, again presumably because they disregard coastal altimetry.

To examine velocity skill on the inner MAB shelf we form an uninterrupted time series of HF-radar observations by averaging data within a 28-km square box near Hudson Canyon (Fig. 1). These data were assimilated in the Doppio reanalysis so it is unsurprising that coherence improves over NA Doppio across all time scales. Coherence with

observations at high frequencies down through the mesoscale is greater than at the PMUI site, which lies beyond the range of MARACOOS HF-radars. While assimilative Doppio shows better multiyear coherence in velocity at the CODAR site, we do not attribute this directly to the assimilation of HF-radar data but rather to the assimilation of coastal altimetry – a claim we base on observation impact analysis (Levin et al., 2021a) of the observing system as a whole.

NERACOOS I01, M01 and N01 (Fig. 1) near-surface current meter observations are used to assess model skill in the coastal and inner (Jordan Basin) GoM and NEC, respectively. The comparison is for alongshore velocity at I01 and M01, and along channel velocity at N01. Subsurface velocity data at I01 and N01 were assimilated in Doppio, but surface currents were not. Since assimilation has improved Doppio's skill more at I01 and N01 than at M01, where no ADCP velocity is assimilated, we speculate that the deep velocity data may have been instrumental in the skill improvement but cannot definitively say it was not altimetry. Mercator and GOFS have little surface current variance in the GoM and are barely coherent with observations.

The Doppio analysis is more skillful at capturing sea level variability than it is surface velocity variability, especially in the mesoscale band, but is considerably better than Mercator and GOFS in capturing variability on all scales.

3.2. Temperature and salinity stratification

The Doppio reanalysis assimilated over 580,000 in situ temperature and 440,000 in situ salinity observations from 2007 to 2021 (Table 3). Most of those observations are present in the Global Telecommunications System (GTS) archives, so GOFS and Mercator assimilate them as well. In Fig. 6, Taylor diagrams show the faithfulness of Doppio, Mercator and GOFS analyses to these assimilated observations, with NA Doppio and MOCHA climatology for added context. On a Taylor diagram the azimuth angle shows correlation, radial distance shows model error standard deviation normalized by observation standard deviation, and normalized RMS error is shown on concentric circles centered on the point (1,0) on the abscissa. A perfect model would fall on the point (1,0), with a ratio of one for the standard deviations, RMS error of zero, and correlation of one. Statistics are computed separately for five geographic subregions shown inset in Fig. 7: Mid Atlantic Bight, Gulf of Maine, Georges Bank, Scotian Shelf, and the deep ocean between the shelf-break and the 3500 m isobath. Statistics are computed on the full daily model fields. The comparison with MOCHA is presented to indicate the skill of a simple data-informed seasonal climatology – a metric that any analysis system should strive to beat. Temperature observations above 20 m depth are excluded from the statistics because the volume of shallow observations tends to overpower the statistics making all correlations close to 1. (All assimilative models have very good skill at capturing near-surface temperature due to assimilation of satellite SST).

Temperature statistics are shown in the upper row of Fig. 6. As might be expected, climatology (asterisks) has less variance than observations (radius less than 1) but captures the seasonal cycle well (correlations from 0.77 on Scotian Shelf to 0.92 in the deep ocean). Non-assimilative Doppio (diamonds) is somewhat more energetic in terms of variability, but is less skillful than climatology in terms of RMS error (RMSE) and correlation. GOFS (pentagonal stars) demonstrates variability on par with observations, but is worse than climatology in terms of correlation and RMSE. Mercator (triangles) is able to improve on climatology in all the metrics, and Doppio is the best of all the models showing very good agreement with these assimilated observations in all regions; all temperature correlations are above 0.9 and the ratio of modeled to observed variance is close to 1.

Salinity statistics are shown in the bottom row of Fig. 6. NA Doppio and GOFS again demonstrate lower correlation and greater RMSE than climatology, while assimilative Doppio matches well the assimilated observations.

Taylor diagrams consider variability only, and do not depict bias. The vertical structure of bias in the upper 200 m of the water column in each subregion is shown in Fig. 7. NA Doppio temperature bias (red lines) is relatively small in the open ocean: within 0.2 °C in the upper 10 m and −0.8 °C at 150 m (red lines in Fig. 7d) but is larger in the coastal areas, and particularly poor on the Scotian Shelf and Georges Bank. Assimilation (blue lines) decreases bias considerably near surface in the GoM and Georges Bank, and somewhat deeper on the Scotian Shelf and MAB. Assimilation is also effective at removing salinity biases (Fig. 7, bottom row), especially the sizeable negative bias near the surface and large positive bias at ~ 100 m in GoM and Georges Bank. Mercator (green lines) and GOFS (black lines) tend to have larger biases than Doppio, particularly in the coastal areas.

For the MAB and Georges Bank, observations between 100 m and 200 m occur only over the steep continental slope. In these regions, Mercator has the lowest deep temperature bias, but why it outperforms Doppio we are unsure. Topographic control of flow is significant in these regions and misrepresentation of the bathymetry could misdirect the sharp contrast in temperature across the shelf-break front. However, the two models represent the steep change in bathymetry at the shelf-break similarly, so other factors must be at play.

Long time series of temperature and salinity at two moorings allow an assessment of the analysis skill for coastal processes in greater detail.

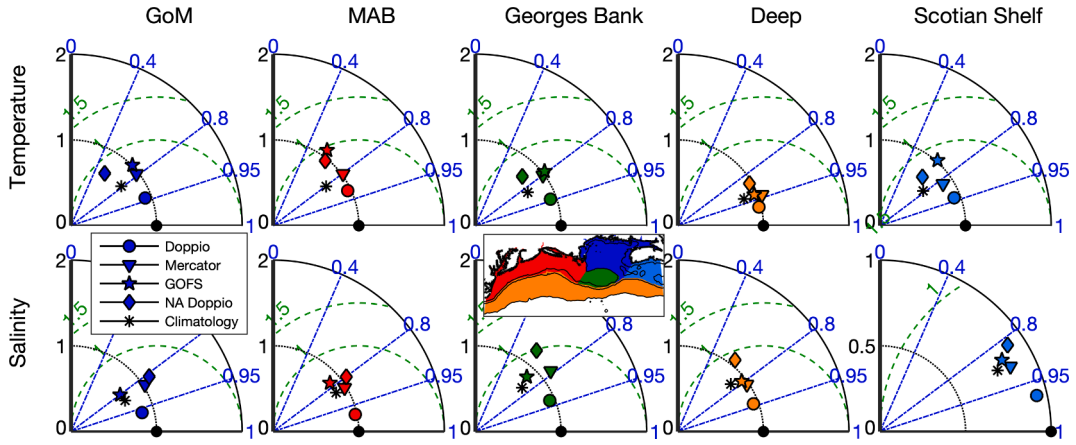

Fig. 6. Taylor diagrams comparing Doppio (circles), Mercator (triangles), GOFS (pentagonal stars), NA Doppio (diamonds), and climatology (asterisks) to observations from subsurface in situ measurements for five subregions indicated in the inset: Gulf of Maine (dark blue symbols), Mid Atlantic Bight (red), Georges Bank (green), Scotian Shelf (light blue), and deep ocean from shelf break to 3500 m isobaths (orange). Top row: temperature. Bottom row: salinity. (For interpretation of the references to color in this figure legend, the reader is referred to the web version of this article.)

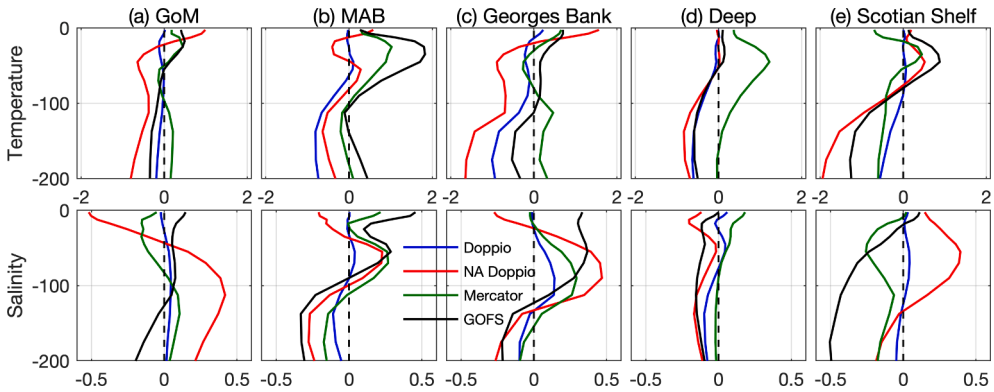

Fig. 7. Vertical structure of upper 200 m mean bias (model minus observations) from Argo floats and ship-based measurements for temperature (°C, upper row), and salinity (g/kg, bottom row) for the five regions outlined in Fig. 6. Doppio (blue), NA Doppio (red), Mercator (green), and GOFS (black). (For interpretation of the references to color in this figure legend, the reader is referred to the web version of this article.)

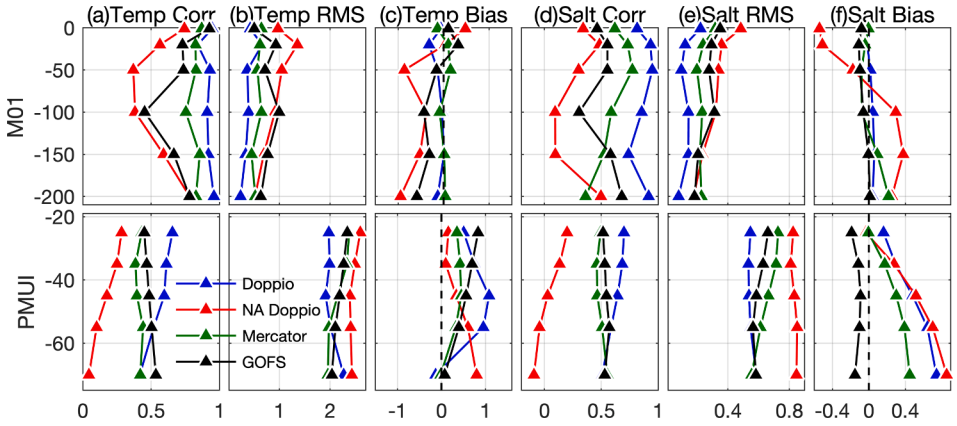

Fig. 8. Comparison of Doppio (blue), Mercator (green), NA Doppio (red) and GOFS (black) with observations from NERACOOS M01 (upper row), and Pioneer PMUI (bottom row). Correlations and RMS errors are computed on anomalies from the seasonal cycle. Bias is the mean of model minus observations. RMSE and bias for temperature and salinity are in °C and g/kg, respectively. Triangles indicate the depths at which statistics were computed. (For interpretation of the references to color in this figure legend, the reader is referred to the web version of this article.)

The NERACOOS M01 buoy gathered hourly T,S observations during most of 2007–2021, and the OOI Pioneer PMUI mooring delivered data during most of 2014–2020. The M01 data were assimilated, but the Pioneer Array observations were not, offering an independent validating data set.

The biases, correlation and RMSE of the respective models compared to mooring observations (after removing the harmonic seasonal cycle) are shown in Fig. 8. Contrasting assimilative and NA Doppio for M01 it is clear that assimilation is able to remove most of the biases present in the NA Doppio solution, especially the negative temperature bias mid column, and a fresh surface salinity bias that stems from weak NEC inflow from the Atlantic. Of the three assimilative models, Doppio has the better correlation and RMSE. Mercator is slightly inferior, while GOFS has good skill in capturing temperature variability near the surface but not deeper in the water column for either variable.

The PMUI mooring data (Fig. 8, bottom row) show that Doppio performs best in term of correlations, and is comparable to Mercator and GOFS for RMSE, but for temperature mid water column and salinity throughout it is biased at this site.

3.3. *Bottom temperature*

To explore the skill at capturing coastal bottom temperatures, we compare to observations collected by NOAA Northeast Fisheries Science

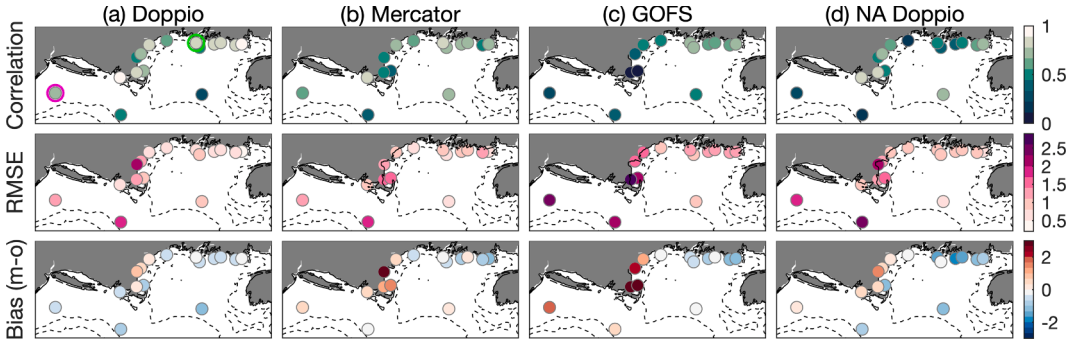

Fig. 9. Comparison of bottom temperature collected by thermistors on NEFSC lobster traps, merged in 20-km bins, during 2007–2021 to models (a) Doppio, (b) Mercator, (c) GOFS, and (d) NA Doppio. Top and center rows: correlations and RMSE (°C) for anomalies from the mean seasonal cycle. Bottom row: mean bias (°C, modeled minus observed). Dashed lines indicate 100 m and 1000 m isobaths. Magenta and green circles show the location of the MAB and GoM sites, respectively, that are used in Fig. 10. (For interpretation of the references to color in this figure legend, the reader is referred to the web version of this article.)

Center (NEFSC) that were not assimilated into any of the models.

NEFSC has collected a large dataset of repeated measurements of bottom temperature from the Environmental Monitors on Lobster Traps (eMOLT) program (Manning and Pelletier, 2014) since 2001. Fig. 9 compares daily-averaged lobster trap measurements with the modeled bottom temperatures. Merging observations in 20-km cells to improve time coverage, we retain time series having more than 2000 days of data for analysis. Correlations and RMSE are computed on anomalies from the mean monthly cycle, while bias is calculated on the full fields.

Generally, all the assimilative models are better correlated with observations in shallower areas (e.g., near the GoM coast) and less skillful in deeper areas (outer MAB shelf and shelf-break). We attribute this to the influence of satellite SST assimilation in shallow waters. Doppio is slightly better than the global models except for RMSE at one site on the GoM coast.

Two particularly long time series in this data set, representative of different coastal regimes, offer more detail about model performance. One site is located on the coast of Maine in 30 m water depth (location is shown by a green circle in upper left plot of Fig. 9) and the other is on the outer MAB shelf in 70 m water depth (magenta circle in Fig. 9).

The mean monthly cycle of observed and modeled bottom temperature at these sites is shown in the top row of Fig. 10. The models adhere well to the observed mean seasonal cycle in the coastal GoM but are less successful on the outer MAB shelf. The 8 °C temperatures at the outer MAB site during Apr-Jun are indicative of the Cold Pool phenomenon (Houghton et al., 1982) wherein waters ventilated during winter in the vicinity of Georges Bank and Nantucket Shoals are capped by intense summer thermal stratification that keeps them largely isolated allowing the low temperatures to persist until overturning of the water column in the fall. Comparing NA Doppio and the reanalysis we see that assimilation improves the winter preconditioning of temperature, and Doppio dynamics subsequently sustain the summer Cold Pool representation through Aug-Sep. However, the Doppio reanalysis is ~ 0.5 °C colder than observed in the fall. Mercator, on the other hand, has a warm bias in the Cold Pool representation, but is closer to observations than Doppio in the fall. In GOFS, temperatures at 70 m are accurate in winter when the water column is fully mixed, but are not preserved when the Cold Pool should form, showing a positive bias of close to 2 °C in summer and fall.

The lower panel of Fig. 10 shows anomalies from the mean monthly cycle smoothed with a 2-month running mean filter. In the coastal GoM (left column) all the models show a clear warming trend over 2007–2021 that is close to the 1.2 °C decade^{-1} during 2005–2017 estimated by Seidov et al. (2021) for the upper 300 m of the entire Gulf of Maine.

Assimilation improves the Doppio correlation and RMS error. The other assimilative models have rather good skill in capturing bottom temperature variability at this site. In common with most of the other skill metrics, the skill of Mercator exceeds that of GOFS but does not quite match Doppio.

Assimilation plays a greater role in improving Doppio's skill at the MAB site (right column of Fig. 10); correlation with observations increases from 0.32 to 0.67 and RMSE decreases from 1.9 °C to 1.4 °C. The GOFS correlation with observations is quite low at 0.26 and RMSE quite large at 3.2 °C. Overall, the models perform less well in the outer MAB than in coastal GoM. For correlations this may be explained in part by the much shorter time series, which allows one or two misrepresented circulation events to carry undue weight. But other metrics have suggested skill decreases with proximity to the shelf edge, and that may be a factor here.

Another independent dataset in shelf waters of the MAB and GoM is some 10,000 near-bottom temperature observations made during 2015–2021 by fishing vessels participating in the NOAA NEFSC Study Fleet (Gawarkiewicz and Malek Mercer, 2019). These data were not assimilated into any of the models. The data are not dense enough to compute meaningful horizontal or vertical statistics, so Fig. 11 shows 2-D histograms (heat maps) of observed temperature versus model interpolated to the same location and time. The overall model biases are

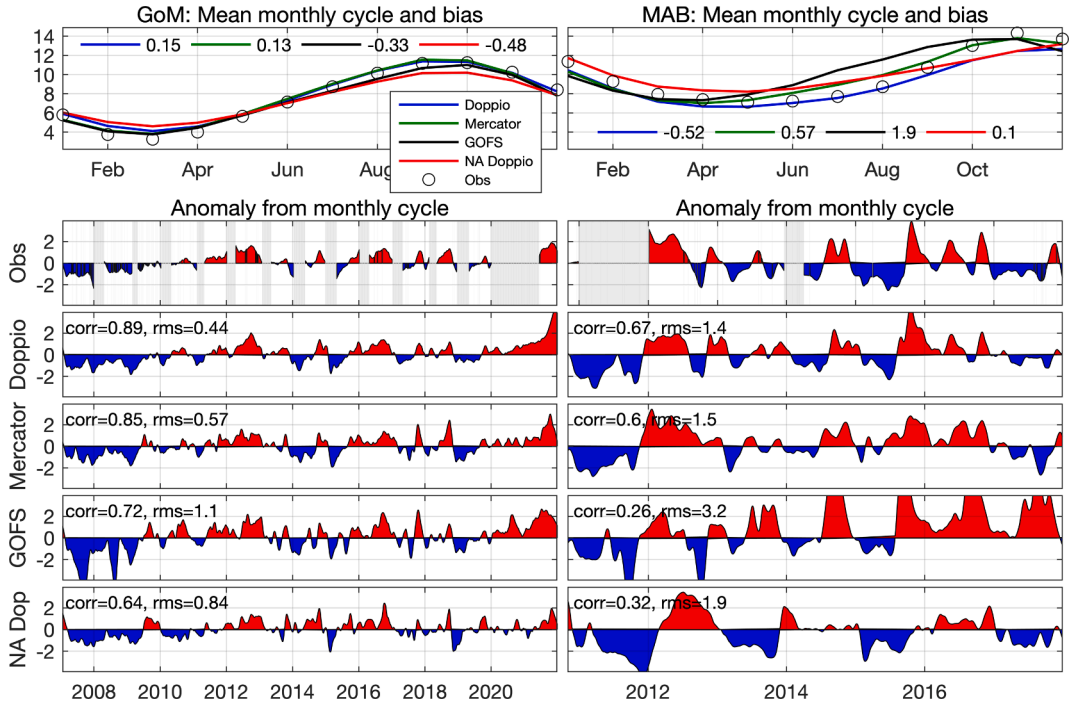

Fig. 10. Comparison of time series of bottom temperature (°C) from NEFSC lobster traps with modeled bottom temperature at two sites: coastal GoM and outer MAB shelf identified in Fig. 9 by green and magenta circles, respectively. Uppermost row: mean seasonal cycle in Doppio (blue line), Mercator (green), GOFS (black), NA Doppio (red) and observations (black circles); annotations note mean bias for each model. Lower panel: time series of 2-month running mean bottom temperature anomalies from the mean seasonal cycle, annotated with correlations and RMSE (before smoothing). Grey areas indicate gaps in the observation time series. (For interpretation of the references to color in this figure legend, the reader is referred to the web version of this article.)

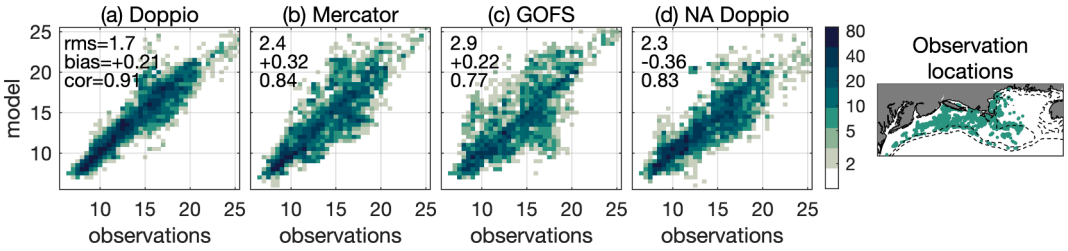

Fig. 11. 2-D histogram of 2015–2021 temperature observations from NEFSC Study Fleet against corresponding modeled temperature at observation location. Color shows the logarithm of the number of observations in 0.5 °C bins. The map at right shows where observations were made.

modest (from −0.36 °C in NA Doppio to +0.32 °C in Mercator), and correlations are generally strong (from 0.77 in GOFS to 0.91 in Doppio), possibly because correlations include seasonal temperature variability (due to the impracticality of removing it from these data). Overall, the Doppio analysis demonstrates the best correlation and RMS error and substantially less spread either side of the one–one line in the range of 6 °C to 12 °C, which is predominantly within the MAB Cold Pool.

3.4. Comparison with independent observations of salinity

Pioneer Array observations were not assimilated into any of the models. These data straddle the MAB shelf-break front that separates relatively fresh shelf waters from more salty Slope Sea waters, and offer insight on performance in this challenging-to-model regime.

Before focusing on salinity, we note that all models compare well with temperature observations (not shown) with correlations of ~ 0.8 on the shelf break (moorings and gliders) and ~ 0.9 in the Slope Sea (gliders only). Since it is not practical to compute a seasonal cycle from these glider observations, statistics are calculated on the full fields. Once again, the Doppio analysis is the best of all the models in RMSE, followed by Mercator, GOFS and NA Doppio.

Comparisons to salinity observations are informative. Some 150,000 salinity observations from gliders and moorings were used in the comparisons shown in Fig. 12. Observations were aggregated in 40-km horizontal bins on standard depths in the vertical, and then compared against corresponding estimates from the models and climatology.

The assimilative models rank in performance as previously, with Doppio having the best correlations and RMSE over the whole area, then Mercator, then GOFS. The biases show an interesting story crossing from the shelf into the Slope Sea. Overall, Doppio has marginally lower biases but with a pronounced pattern of warm bias inside the shelf-break front yet cool offshore. This is consistent with an under-resolved frontal boundary. Mercator exhibits a similar pattern but with elevated magnitude. GOFS has a large cool bias throughout. MOCHA climatology, based entirely on data acquired prior to 2009, presents as cool by more than 0.25 °C compared to the more recent Pioneer data, consistent with recognized region-wide climate warming trends. We have not endeavored to unpack how vertical structure plays into these skill metrics, but Fig. 8 suggests errors are most pronounced below 50 m.

To delve deeper into salinity skill, we utilize surface salinity observed by the Soil Moisture Active Passive (SMAP) V4 satellite (Meissner et al., 2019) as another independent dataset. SMAP data are rather noisy and known to have issues near the coast due to land contamination in the radiometer field of view, but have been proven to have skill in capturing mesoscale variability (Grodsky et al., 2018a) on monthly time scales. Correlation, RMSE and bias between monthly average model outputs and SMAP estimates for 2015–2021 are shown in Fig. 13 based on anomalies from the mean seasonal cycle to emphasize mesoscale variability. Biases are computed from the full fields. NA Doppio (Fig. 13d) has a considerable fresh bias in the GoM and MAB, which we attribute to model resolution hampering inflow to the GoM of salty North Atlantic water through an under-resolved Northeast Channel. Furthermore, the GoM coastal current is too diffuse and allows fresh water from rivers to spread into the interior GoM. Unlike the results for Pioneer Array salinity (Fig. 12), there is no discernible decrease in skill at the MAB shelf break, agreeing with our previous assertion that the problems the models have with salinity at the shelf break are predominantly subsurface.

All the models show a salty bias in the Slope Sea immediately north of Cape Hatteras, indicating a slight overshoot of the Gulf Stream separation. The low correlation for Doppio in the Gulf Stream area might raise concerns over proximity to the open boundary, but Mercator and GOFS show similar or worse correlations, so this may simply stem from the lack of signal variance there: SSS is consistently salty.

Doppio and Mercator show substantial skill in capturing SSS mesoscale variability in the Slope Sea, and reasonable skill in the MAB; both outperform GOFS. They also have less bias in the Slope Sea than GOFS (Fig. 13a-c). Doppio and Mercator show a fresh SSS bias in coastal areas. However, as we show next, examination of vessel thermosalinograph (TSG) data suggests this may reflect an issue in SMAP itself.

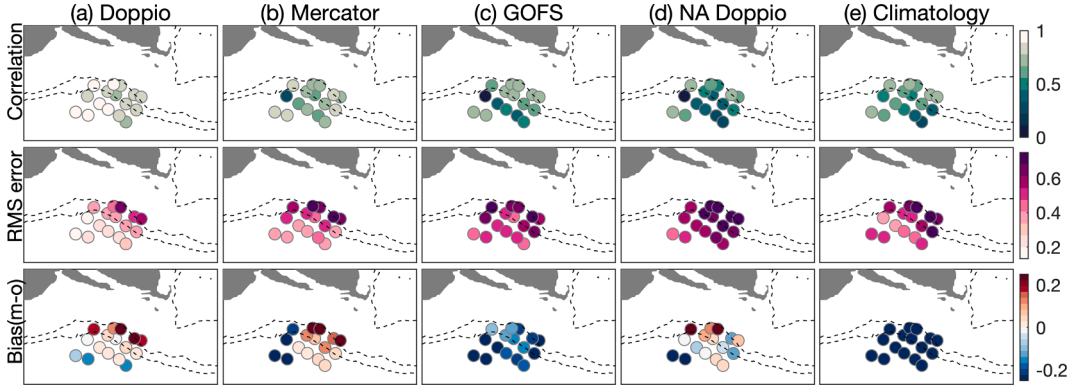

Fig. 12. Comparison between salinity from 2014 to 2020 Pioneer gliders and moorings and corresponding salinity in (a) Doppio, (b) Mercator, (c) GOFS, (d) NA Doppio and (e) MOCHA Climatology. Model values were interpolated to the observation location in space and time, and aggregated in half-degree cells. Top row: correlations. Middle row: RMS error. Bottom row: mean bias (model minus observed). Dashed lines indicate 100-m and 1000-m isobaths.

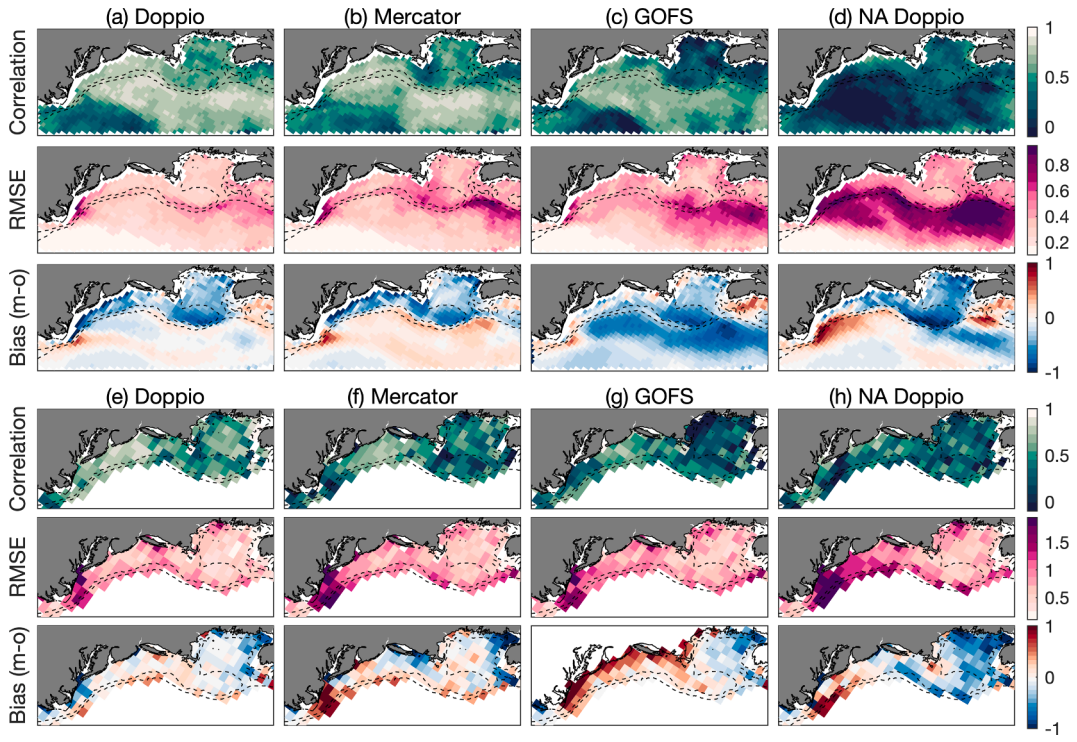

Fig. 13. Comparison between 2015 and 2021 SMAP SSS with (a) Doppio, (b) Mercator, (c) GOFS and (d) NA Doppio; and comparison between 2009 and 2021 SSS from TSG with (e) Doppio, (f) Mercator, (g) GOFS and (h) NA Doppio. Cross-correlations and RMS errors are computed on anomalies from the seasonal cycle; bias is the mean difference of model minus observations. Bias and RMSE in g/kg.

There is a wealth of salinity data in the MAB, GoM and on Georges Bank from TSG on the NOAA vessels Bigelow, Gunter and Pisces (Wang 2017). While some of these data are in the GTS and UKMO EN4 databases, and are assimilated in all the models, we found around 2.5 million observations during 2009–2021 that are not in those archives that are sufficient to compute anomalies from the seasonal cycle in adequately resolved spatial bins (Fig. 13e-h). The Doppio and Mercator biases for these independent TSG data are much smaller than for the SMAP comparison suggesting that the bias we reported in coastal regions should be taken with a grain of salt. This brings into question the low coastal bias in GOFS compared to SMAP; there is now a large positive (salty) bias near the MAB and GoM coast when GOFS is compared to TSG.

This comparison to independent TSG SSS observations indicates Doppio is the most skillful, with Mercator also performing well in the open ocean and MAB. However, all models struggle to capture Gulf of Maine salinity variability.

3.5. Coastal ocean response to hurricane Irene

Hurricane Irene traversed the MAB shelf during 27–29 August 2011 (green line in Fig. 14) with high winds that caused vigorous vertical mixing. At this time of year stratification on the MAB shelf is still strong and the Cold Pool is intact (Seroka et al., 2017), so mixing brought anomalously cold and salty water to the surface lowering SST by some 6 °C. The drop in temperature was so severe that our observation quality control algorithms had to be adjusted in order not to reject the unusually cold satellite SST observations. The change in SST averaged over three days preceding and following the passage of Irene is shown in Fig. 14. There is a pronounced drop in temperature throughout the MAB in all models, though to a lesser degree in Mercator. Irene also brought about a shelf-wide increase in SSS of 0.5 g/kg in both Doppio and Mercator while GOFS, on the other hand, exhibited freshening in the wake of the storm.

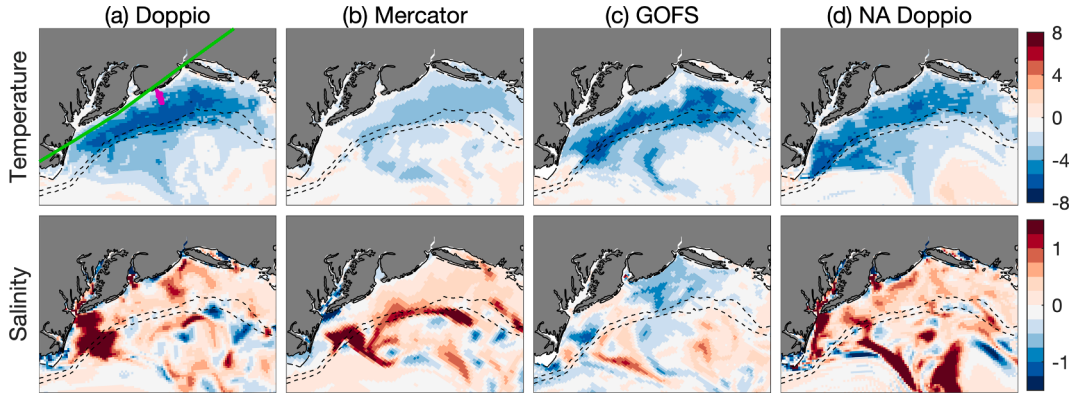

Fig. 14. The change in temperature (°C, top row) and salinity (g/kg, bottom row) brought by Irene, as a difference between Aug. 29–31 mean (after Irene) and Aug. 23–26 mean (before Irene). The glider track is shown by a magenta line and the hurricane track by a green line in the upper left plot. (For interpretation of the references to color in this figure legend, the reader is referred to the web version of this article.)

We are able to better understand the modeled response to the storm by examining the vertical structure of temperature and salinity pre- and post-Irene in comparison to data from an IOOS glider that was present close to Irene's path in late August 2011 (glider track is shown by the magenta line in Fig. 14). The glider observations and model fields at their native vertical resolution interpolated to the horizontal coordinates of the glider track are shown in Fig. 15. These data were assimilated in Doppio. In 2011, IOOS glider data were not yet being transmitted to GTS and were not assimilated into these versions of Mercator or GOFS.

Even without assimilation, NA Doppio captured well the sharp summer thermocline and halocline prior to the storm, especially the ~ 10 °C waters of the Cold Pool, but did not realize the observed cooling. Assimilation removed the fresh bias of NA Doppio in the Cold Pool, decreasing water column stability and presumably allowing mixing to extend deeper down to 20 m instead of 10 m, thereby bringing cooler waters to the surface.

The difference between Doppio and the two global models is pronounced. The lack of vertical resolution in GOFS (fewer than five points) limits its ability to resolve stratification so close to the coast. The Cold Pool is absent, so storm-induced mixing does not have a reservoir of cold water to entrain into the surface layer and surface cooling in GOFS is presumably due to assimilation of SST. Mercator vertical resolution is better than GOFS but not as fine as the terrain-following coordinate of Doppio. Mercator appears to over-mix the water column, starting from conditions that are much less stable than observed; the mixed layer is deeper, the thermocline more diffuse, and the Cold Pool is too weak; the surface waters are too salty. On Aug. 25 and Aug. 30, the glider was close to the coast (the profiles are only 20 m deep) and the observed salinity was as low as 30 g/kg. Both Doppio models captured this low salinity feature that was the result of significant fresh water input from rivers during the storm, but this signal is missing from the two global models.

3.6. Salinity anomalies in the Gulf of Maine

Unusually high surface salinities of 34 g/kg were observed in the GoM during Jan.-Feb. 2018 by SMAP (Grodsky et al., 2018a). In Fig. 16 we show the difference of observed and modeled SSS from their respective mean seasonal cycles (to reduce the effects of possible bias in SMAP noted in section 3.4). The positive salinity anomaly is captured in both Doppio models and Mercator, but is barely noticeable in GOFS. This unusual salinification has been attributed to the combination of a warm and salty horizontal intrusion from a summer-fall 2017 Gulf Stream Warm Core Ring (WCR) event (Grodsky et al., 2018b; Gonçalves Neto et al., 2021) and vertical mixing due to the loss of stratification caused by a drastic reduction of surface fresh water input from the Scotian Shelf (Levin et al., 2022).

This strong vertical mixing event, captured by six fixed depth T,S sensors at NERACOOS buoy M01 (Fig. 17), was quite anomalous in the long historical record at this site (not shown). The observations show deep pulses of unusually salty water at 200 m in Oct.-Nov. 2017 and Jan.-Feb. 2018. Near the surface (20 m depth), water of elevated salinity (34 g/kg) appeared in Feb. 2018. Variational data assimilation dynamically interpolates between the sensors to reconstruct the changes in stratification during the six months prior to the event. All the models start from a well-stratified water column in Sep. 2017, but show varying representations of the vertical mixing in Jan. 2018 that brings deep salty water to the surface. Only Doppio is able to reconstruct both unusual subsurface mixing down to 100 m as well as the pulses of salty water at depth. The bias in NA Doppio is severe, being too fresh at the surface and too salty at depth resulting in an overly stratified water column and weak mixing.

NERACOOS mooring data are transmitted to the Global Telecommunications System (GTS) and are therefore acquired for assimilation by the global models. Mercator captures the vertical mixing that raises SSS to 34 g/kg, but misses the deep (200 m) warm and salty water intrusions. GOFS exhibits the deep high salinity values but not the deep mixing. Compared to Doppio, the early fall thermocline and halocline are too deep and diffuse in Mercator and GOFS, and GOFS fields are rather noisy. However, it should be said that the performance of Mercator is outstanding for a global modeling and analysis system that does not include explicit tides, which are famously strong in the GoM.

Returning to Fig. 16, two distinctive positive salinity anomalies in the Atlantic Slope Sea contribute to the two pulses of warm and salty water at M01. One is a WCR with its eye positioned near the Northeast Channel in Jul. 2017; the second is associated with another, weaker WCR in Nov.-Dec. with its eye south of the NEC (Levin et al., 2022). A 3-month advective transport lag for these two anomalies to penetrate from the NEC into the inner GoM and reach M01 in Oct.-Nov. 2017 and Feb. 2018, respectively, is consistent with the study of Du et al. (2021).

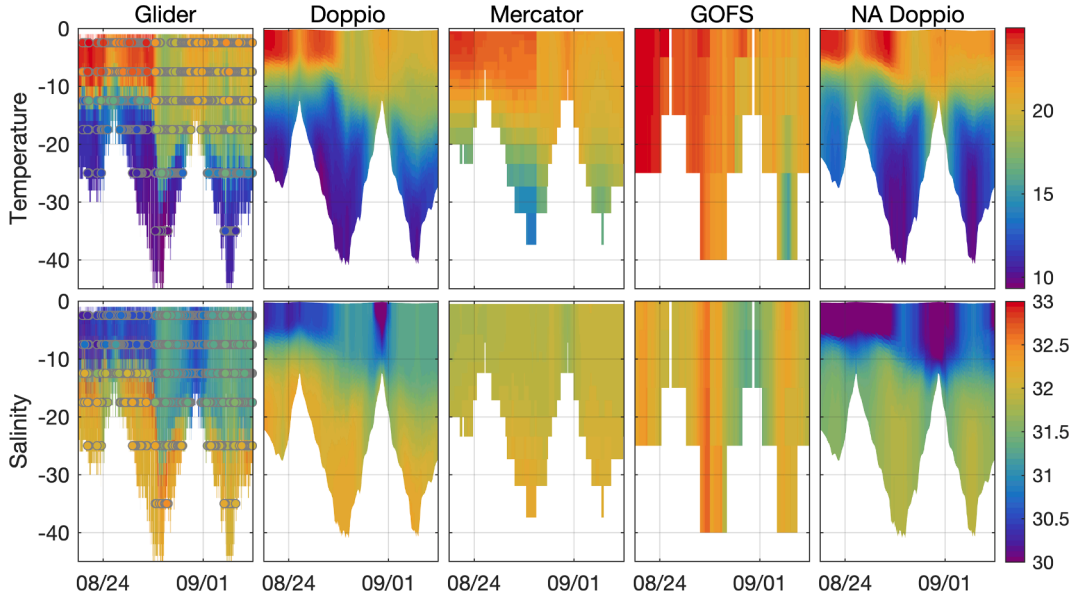

Fig. 15. Comparison of Doppio, Mercator, GOFS and NA Doppio models with glider observations of temperature (°C) (upper row) and salinity (g/kg) (lower row) collected before and during hurricane Irene (Aug.-Sep. 2011). Colored circles show binned observations that were assimilated. Model transects are taken along the glider path.

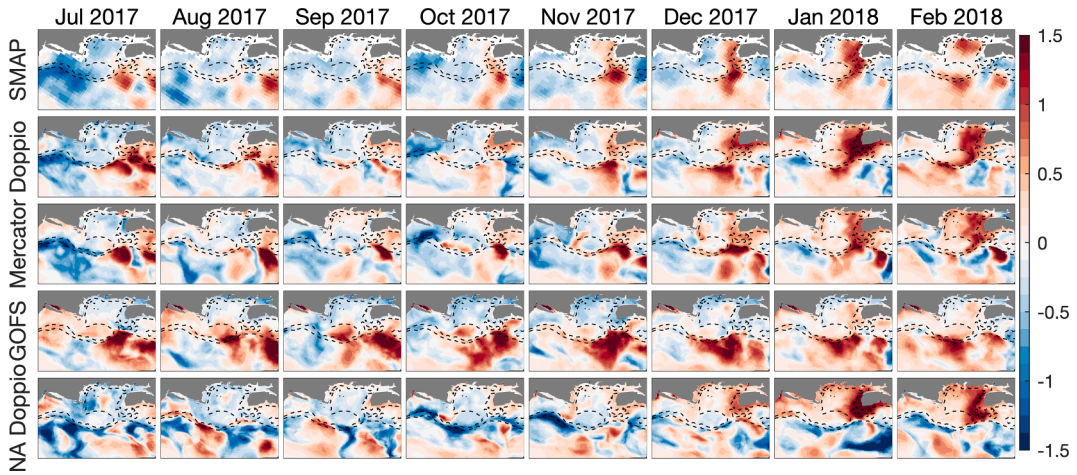

Fig. 16. Monthly SSS anomaly (g/kg) from respective 2015–2021 mean seasonal cycles during July 2017 to March 2018 from SMAP, Doppio, Mercator, GOFS and NA Doppio.

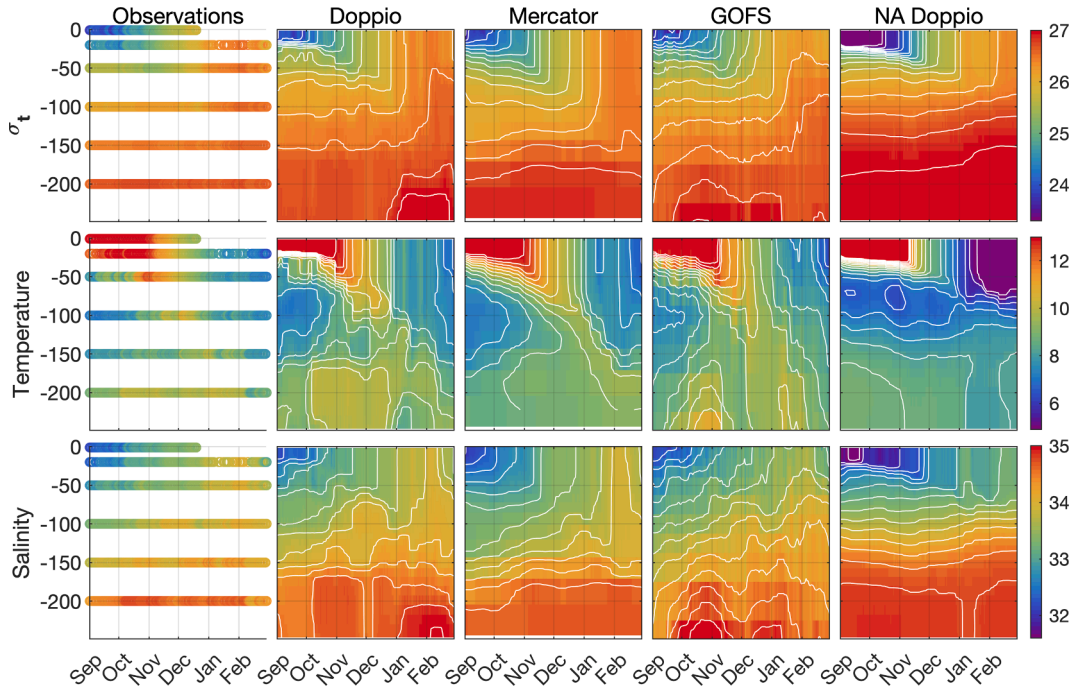

Fig. 17. Comparison of Doppio, Mercator, GOFS, and NA Doppio models and observations at NERACOOS buoy site M01. Time series of (top row) density σ_t (kg m^{-3}), (center row) temperature (°C) and (bottom row) salinity (g/kg) during Sep. 2017 to Mar. 2018.

4. Summary

We have described the configuration and performance of the "Doppio" data assimilative regional ocean modeling system that downscales output from the Mercator-Océan global model and assimilates additional local observations. Key elements of the system are (i) a regional ROMS ocean model encompassing major estuaries and shallow coastal waters of the Mid-Atlantic Bight and Gulf of Maine and extending far enough offshore to enable representation of oceanic mesoscale variability in the Gulf Stream that impacts coastal circulation, (ii) accurate surface meteorological forcing, (iii) attention to representing daily variability in the buoyancy input from coastal river inflows, (iv) preprocessing to decrease biases in open boundary conditions by reference to a local, high resolution ocean hydrographic climatology, (v) a data assimilative analysis of climatological mean observations constrained by model dynamics and kinematics to obtain balanced open boundary mean velocities and a consistent regional Mean Dynamic Topography to augment satellite altimeter sea level anomaly data during assimilation, (vi) assembly of a 15-year-long comprehensive suite of remote and in situ regional observations from all available platforms, and (vii) assimilation of these observations by 4D-Var. Additional data sources that are not assimilated are used for independent assessment of the system skill.

The key choices made in configuring ROMS for the dynamical regime of the MAB and GoM region are noted, and a brief overview of ROMS 4D-Var and how we have configured it for Doppio are provided. We have documented the observing platforms and data sources accessed, our data pre-processing and quality control approaches, and justified the error hypotheses used to implement a 4D-Var system suited to a coastal environment. These aspects are described in some detail for users who might wish to emulate our efforts and develop similar model downscaling systems for other coastal regions globally.

Performance of the Doppio model reanalysis has been assessed by examining the fit to assimilated data, and by comparison to independent unassimilated observations from coastal tide gauges, Pioneer Array gliders and moorings, SMAP satellite SSS, in situ TSG salinity, and sensors deployed on fishing gear. Most assessments employ statistical analyses of daily model fields and long observational time series available for 2007–2021. Anticipating the interests of stakeholder communities in coastal inundation and ecosystems, the independent skill assessments direct particular focus on coastal sea level variability and bottom temperatures.

The Doppio analysis of sea level variability is highly coherent with tide gauge data throughout the domain and across all time scales from annual to daily, an achievement we credit largely to the assimilation of coastal altimetry data. The analysis outputs are, therefore, a strong candidate for setting sub-tidal frequency open boundary conditions for models that further downscale dynamics into estuaries and back bays (e.g., Defne and Ganju, 2015).

Bottom temperatures on the continental shelf exert significant influence on benthic ecosystems, including commercial fisheries (Munroe et al., 2016; Fredston et al., 2021). Our assessment of the modeled temperatures at precisely the location of fishing activity, using data generously collected by the Northeast Study Fleet and eMOLT programs, indicates appreciable skill in capturing geographic patterns and mesoscale, seasonal and inter-annual temporal variability.

We are optimistic that the ocean circulation reanalysis products described here will prove useful for studies of the influence of ocean circulation on regional biogeochemistry and the MAB and GoM Large Marine Ecosystem. As an example, the Doppio analysis has already been adopted to constrain shelf-wide conditions in a nested ROMS model of the Delaware Bay to examine estuarine retention of invertebrate larvae (Garwood et al., 2022).

The analysis skill in depicting particular ocean circulation events was demonstrated by examining the impacts of Hurricane Irene (Aug. 2011) on vertical stratification in the MAB; and the effects of Gulf Stream Warm Core Ring and Scotian Shelf inflow on stratification in the GoM in the fall and winter of 2017–2018.

To show the impact of assimilation, as opposed to downscaling, results from the assimilative Doppio analysis were compared with results from an equivalent, free-running non-assimilative Doppio model. The former improves on the latter both in terms of mean circulation and variability throughout the model domain, especially at the ocean mesoscale. Skill is not significantly enhanced at periods shorter than a few days, but the Doppio model is already quite skillful at high frequencies and this is not adversely impacted by assimilation.

To show the value added by local downscaling, results from two OceanPredict assimilative global ocean models were compared to the Doppio analysis. Whether compared to assimilated or independent observations, the assimilative Doppio system performed better than Mercator, and especially GOFS, throughout the MAB and GoM with respect to skill metrics for all the ocean state variables: sea level, velocity, temperature and salinity.

Global operational forecasts and reanalysis products such as from Mercator-Océan are invaluable tools for mesoscale applied oceanography, but they do not yet rise to the level of skill on many continental shelves with respect to currents, sea level, and bottom temperatures that is required to best support coastal applications. This paper has built a strong case for the value of undertaking regional downscaling of global systems, with added data assimilation, to provide more skillful estimates of ocean circulation in coastal, shelf and adjacent deep ocean waters.

A particular strength of the approach taken here is the synergy of deriving a regional, dynamically balanced, data-informed climatological mean circulation analysis both for correcting biases in the global analyses to be downscaled but also for enabling the greater use of altimeter data up to the coast. While AVISO global Mean Dynamic Topography (MDT) products have improved markedly in recent years (Mulet et al. 2021), they still exhibit weak or dynamically unphysical patterns on broad continental shelves and adjacent to the coast that hampers their utility for many coastal circulation applications (Feng et al., 2018).

There remains, however, ample scope for further improving the analysis here. We see decreased skill near the continental shelf edge with respect to bottom temperatures, which we attribute to poor resolution of the bathymetry there. Lack of resolution of the Northeast Channel is also implicated in hampering accurate realization of the exchange flow into and out of the Gulf of Maine. These issues can be addressed with a higher resolution ROMS model, though with the attendant added computational cost of 4D-Var.

Shelf edge bottom temperatures would also be improved by assimilation of the fishing fleet and eMOLT data that were withheld here. Likewise, assimilation of SMAP and TSG salinity data has the potential to improve the modeled water mass properties, though to do so we would first need to reconcile the offset in near coastal SMAP salinity versus in situ observations.

Were these data sets to be assimilated in a new version of the Doppio reanalysis, there would remain rather little independent data to quantify whether the hoped-for skill improvement was realized. Drawing on standard practice in Numerical Weather Prediction, an approach would be to treat each 3-day prior analysis as a forecast, and the converged 4D-Var solution as a verifying analysis, and quantify the change in skill compared to the analysis product presented here. Both an enhanced resolution underlying model, and an expansion in the data sets assimilated, are developments we are pursuing.

Outputs from the 15-year reanalysis are available for download via a THREDDS (Thematic Real-time Environmental Distributed Data Services) web service to facilitate user geospatial or temporal sub-setting. Results are provided on the ROMS model native 3-dimensional grid as (i) 1-hourly interval snapshots, (ii) 1-day averages, (iii) monthly averages, (iv) yearly averages, and (v) ensemble monthly averages (i.e., the mean of all days in the same month from all years). ROMS outputs are in netCDF format with data and metadata that follow CF-1.4 Conventions for the description of coordinates and variables. The preprocessed observations that were assimilated and their provenance, prior and posterior errors, and corresponding values interpolated from the global models, are accessible via an ERDDAP web service. Example ROMS output files for direct download and hyperlinks to the THREDDS catalog and observations ERDDAP end-points are given by Wilkin and Levin (2022).

CRediT authorship contribution statement

John Wilkin: Conceptualization, Methodology, Validation, Writing – original draft, Supervision, Project administration, Funding acquisition. **Julia Levin:** Methodology, Software, Validation, Formal analysis, Investigation, Writing – original draft, Visualization. **Andrew Moore:** Conceptualization, Methodology, Supervision. **Hernan Arango:** Methodology, Software, Investigation, Supervision. **Alexander López:** Conceptualization, Methodology, Software, Validation, Investigation. **Elias Hunter:** Software, Data curation.

Declaration of Competing Interest

The authors declare that they have no known competing financial interests or personal relationships that could have appeared to influence the work reported in this paper.

Data availability

Open data access is described at SEANOE https://www.seanoe.org/data/00785/89673.

Acknowledgements

This work was funded by NOAA [award NA16NOS0120020], NASA [award NNX17AH58G] and NSF [award 1459646].

References

Becker, J.J., Sandwell, D.T., Smith, W.H.F., Braud, J., Binder, B., Depner, J., Fabre, D., Factor, J., Ingalls, S., Kim, S.-H., Ladner, R., Marks, K., Nelson, S., Pharaoh, A., Trimmer, R., Von Rosenberg, J., Wallace, G., Weatherall, P., 2009. Global bathymetry and elevation data at 30 arc seconds resolution: SRTM30_PLUS. Mar. Geod. 32 (4), 355–371.

Bell, M., Schiller, A., Le Traon, P., Smith, N., Dombrowsky, E., Wilmer-Becker, K., 2015. An introduction to GODAE OceanView. J. Operat. Oceanogr.. 8 (sup1), s2–s11. https://doi.org/10.1080/1755876X.2015.1022041.

Blayo, E., Debreu, L., 2006. Nesting Ocean Models. In: Chassignet, E.P., Verron, J. (Eds.), OceAn Weather Forecasting: An Integrated View of OceAnography. Springer, pp. 127–146.

Boyer, T.P., Antonov, J.I., Baranova, O.K., Garcia, H.E., Johnson, D.R., Locarnini, R.A., Mishonov, A.V., O'Brien, T.D., Seidov, D., Smolyar, I.V., Zweng, M.M., 2009. World Ocean Database 2009, S. Levitus, Ed., NOAA Atlas NESDIS 66, U.S. Government Printing Office, Washington, D.C., 216 pp., DVDs.

Chassignet, E., Hurlburt, H., Metzger, E.J., Smedstad, O., Cummings, J., Halliwell, G., Bleck, R., Baraille, R., Wallcraft, A., Lozano, C., Tolman, H., Srinivasan, A., Hankin, S., Cornillon, P., Weisberg, R., Barth, A., He, R., Werner, F., Wilkin, J., 2009. U.S. GODAE: global ocean prediction with the HYbrid coordinate ocean model (HYCOM). Oceanography 22 (2), 64–75.

Cipollini, P., Benveniste, J., Birol, F., Fernandes, M.J., Obligis, E., Passaro, M., Strub, P. T., Valladeau, G., Vignudelli, S., Wilkin, J., 2017. Satellite Altimetry in Coastal Regions. In: Stammer, D., Cazenave, A. (Eds.), Satellite Altimetry Over Oceans and Land Surfaces. CRC Press, Boca Raton, pp. 343–380.

Csanady, G.T., 1976. Mean circulation in shallow seas. J. Geophys. Res. 81 (30), 5389–5399.

Daley, R., 1991. Atmospheric Data Analysis. Cambridge University Press, p. 472 pp..

Dalyander, P.S., Butman, B., Sherwood, C.R., Signell, R.P., Wilkin, J.L., 2013. Characterizing wave-and current-induced bottom shear stress: US middle Atlantic continental shelf. Continent. Shelf Res. 52, 73–86.

Defne, Z., Ganju, N.K., 2015. Quantifying the residence time and flushing characteristics of a shallow, back-barrier estuary: application of hydrodynamic and particle tracking models. Estuaries Coasts 38 (5), 1719–1734.

Desroziers, G., Berre, L., Chapnik, B., Poli, P., 2005. Diagnosis of observation, background and analysis-error statistics in observation space. Q. J. R. Meteorol. Soc. 131, 3385–3396.

Du, J., Zhang, W.G., Li, Y., 2021. Variability of deep water in jordan basin of the gulf of maine: influence of gulf stream warm core rings and the nova scotia current. e2020JC017136 J. Geophys. Res.: Oceans. 126 (5). https://doi.org/10.1029/2020JC017136.

Egbert, G.D., Erofeeva, S.Y., 2002. Efficient inverse modeling of barotropic ocean tides. J. Atmos. Oceanic Technol. 19 (2), 183–204. https://doi.org/10.1175/1520-0426(2002)019<0183:EIMOBO>2.0.CO;2.

Fairall, C.W., Bradley, E.F., Hare, J.E., Grachev, A.A., Edson, J.B., 2003. Bulk parameterization of air-sea fluxes: updates and verification for the COARE algorithm. J. Clim. 16 (4), 571–591. https://doi.org/10.1175/1520-0442(2003)016<0571:BPOASF>2.0.CO;2.

Feng, H., Vandemark, D., 2011. Altimeter data evaluation in the coastal gulf of Maine and mid-Atlantic bight regions. Ma. Geod. 34 (3–4), 340–363. https://doi.org/10.1080/01490419.2011.584828.

Feng, H., Vandemark, D., Levin, J., Wilkin, J., 2018. Examining the accuracy of GlobCurrent upper ocean velocity data products on the Northwestern atlantic shelf. Remote Sens. 10 (8), 1205. https://doi.org/10.3390/rs10081205.

Fleming, N.E., 2016. Seasonal and spatial variability in temperature, salinity and circulation of the Middle Atlantic Bight, PhD, 336 pp, Rutgers University, New Brunswick, NJ 10.7282/T3XW4N4M.

Fratantoni, P., Pickart, R., 2003. Variability of the shelf break jet in the Middle Atlantic Bight: Internally or externally forced. J. Geophys. Res. 108, 3166.

Fredston, A., Pinsky, M., Selden, R.L., Szuwalski, C., Thorson, J.T., Gaines, S.D., Halpern, B.S., 2021. Range edges of North American marine species are tracking temperature over decades. Global Change Biol. 27 (13), 3145–3156.

Garwood, J., Fuchs, H., Gerbi, G., Hunter, E., Chant, R., Wilkin, J., 2022. Estuarine retention of larvae: contrasting effects of behavioral responses to turbulence and waves. Limnol. Oceanogr. 67, 992–1005. https://doi.org/10.1002/lno.12052.

Gawarkiewicz, G., Brink, K., Bahr, F., Beardsley, R., Caruso, M., Lynch, J., Chiu, C., 2004. A large-amplitude meander of the shelfbreak front during summer south of New England: observations from the Shelfbreak PRIMER experiment. J. Geophys. Res. Oceans. 109, C03006. https://doi.org/10.1029/2002JC001468.

Gawarkiewicz, G., Malek Mercer, A., 2019. Partnering with fishing fleets to monitor ocean conditions. Ann. Rev. Mar. Sci. 11 (1), 391–411. https://doi.org/10.1146/annurev-marine-010318-095201.

Gonçalves Neto, A., Langan, J.A., Palter, J.B., 2021. Changes in the Gulf Stream preceded rapid warming of the Northwest Atlantic Shelf. Commun. Earth Environ. 2 (1), 74. https://doi.org/10.1038/s43247-021-00143-5.

Good, S.A., Martin, M.J., Rayner, N.A., 2013. EN4: quality controlled ocean temperature and salinity profiles and monthly objective analyses with uncertainty estimates. J. Geophys. Res.: Oceans. 118, 6704–6716. https://doi.org/10.1002/2013JC009067.

Grodsky, S., Vandemark, D., Feng, H., 2018a. Assessing coastal SMAP surface salinity accuracy and its application to monitoring gulf of Maine circulation dynamics. Remote Sens. 10 (8), 1232. https://doi.org/10.3390/rs10081232.

Grodsky, S.A., Vandemark, D., Feng, H., Levin, J., 2018b. Satellite detection of an unusual intrusion of salty slope water into a marginal sea: Using SMAP to monitor Gulf of Maine inflows. Remote Sens. Environ. 217, 550–561.

Gürol, S., Weaver, A., Moore, A., Piacentini, A., Arango, H., Gratton, S., 2014. B-preconditioned minimization algorithms for variational data assimilation with the dual formulation. Quart. J. R. Meteorol. Soc. 140, 539–556. https://doi.org/10.1002/qj.2150.

Houghton, R.W., Schlitz, R., Beardsley, R.C., Butman, B., Chamberlin, J.L., 1982. The middle Atlantic bight cold pool: evolution of the temperature structure during summer 1979. J. Phys. Oceanogr. 12 (10), 1019–1029.

Hu, J., Fennel, K., Mattern, J.P., Wilkin, J., 2012. Data assimilation with a local Ensemble Kalman Filter applied to a three-dimensional biological model of the Middle Atlantic Bight. J. Mar. Syst. 94, 145–156. https://doi.org/10.1016/j.jmarsys.2011.11.016.

Janeković, I., Mihanović, H., Vilibić, I., Grčić, B., Ivatek-Šahdan, S., Tudor, M., Djakovac, T., 2020. Using multi-platform 4D-Var data assimilation to improve modeling of Adriatic Sea dynamics. Ocean Model. 146, 101538.

Kerry, C., Powell, B., Roughan, M., Oke, P., 2016. Development and evaluation of a high-resolution reanalysis of the East Australian Current region using the Regional Ocean Modelling System (ROMS 3.4) and Incremental Strong-Constraint 4-Dimensional Variational (IS4D-Var) data assimilation. Geoscientific Model Dev. 9 (10), 3779–3801.

Lee, J.H., Kim, T., Pang, I.C., Moon, J.H., 2018. 4DVAR data assimilation with the regional ocean modeling system (ROMS): impact on the water mass distributions in the Yellow Sea. Ocean Sci. J. 53 (2), 165–178.

Lellouche, J.-M., Le Galloudec, O., Regnier, G., Levier, B., Greiner E., Drévillon, M., 2019. Quality Information Document for Global Sea Physical Analysis and Forecasting Product. Copernicus Marine Environmental Monitoring Service report CMEMS-GLO-QUID-001-024, pp. 81, https://catalogue.marine.copernicus.eu/documents/QUID/CMEMS-GLO-QUID-001-024.pdf.

Lellouche, J.-M., Greiner, E., Le Galloudec, O., Garric, G., Regnier, C., Drévillon, M., Benkiran, M., Testut, C.-E., Bourdallé-Badie, R., Gasparin, F., Hernandez, O., Levier, B., Drillet, Y., Remy, E., Le Traon, P.-Y., 2018. Recent updates to the Copernicus Marine Service global ocean monitoring and forecasting real-time 1/12° high-resolution system. Ocean Sci. 14, 1093–1126. https://doi.org/10.5194/os-14-1093-2018.

Lentz, S., 2008a. Observations and a model of the mean circulation over the middle Atlantic bight continental shelf. J. Phys. Oceanogr. 38, 1203–1221. https://doi.org/10.1175/2007JPO3768.1.

Lentz, S., 2008b. Seasonal variations in the circulation over the Middle Atlantic Bight continental shelf. J. Phys. Oceanogr. 38, 1486–1500.

Levin, J., Wilkin, J., Fleming, N., Zavala-Garay, J., 2018. Mean circulation of the Mid-Atlantic Bight from a climatological data assimilative model. Ocean Model. 128, 1–14. https://doi.org/10.1016/j.ocemod.2018.05.003.

Levin, J., Arango, H.G., Laughlin, B., Hunter, E., Wilkin, J., Moore, A.M., 2020. Observation impacts on the Mid-Atlantic Bight front and cross-shelf transport in 4D-Var ocean state estimates, Part I - Multiplatform Analysis. Ocean Model. 156, 101721 https://doi.org/10.1016/j.ocemod.2020.101721.

Levin, J., Arango, H.G., Laughlin, B., Wilkin, J., Moore, A.M., 2021a. The impact of remote sensing observations on cross-shelf transport estimates from 4D-var analyses of the mid-atlantic bight. Adv. Space Res. 68, 553–570. https://doi.org/10.1016/j.asr.2019.09.012.

Levin, J., Arango, H., Laughlin, B., Hunter, E., Wilkin, J., Moore, A., 2021b. Observation impacts on the mid-atlantic bight front and cross-shelf transport in 4D-var ocean state estimates, Part II – The Pioneer Array. Ocean Model. 157, 101731 https://doi.org/10.1016/j.ocemod.2020.101731.

Levin, J.C., Grodsky, S.A., Vandemark, D., Wilkin, J.L., 2022. Haline control of unusually deep winter mixing in the gulf of maine investigated using a regional data-assimilative model. Earth Space Sci. Open Archive 35. https://doi.org/10.1002/essoar.10509004.1.

Linder, C.A., Gawarkiewicz, G., 1998. A climatology of the shelfbreak front in the Middle Atlantic Bight. J. Geophys. Res. 103 (C9), 18405–18423.

López, A.G., Wilkin, J.L., Levin, J.C., 2020. Doppio – a ROMS (v3.6)-based circulation model for the Mid-Atlantic Bight and Gulf of Maine: configuration and comparison to integrated coastal observing network observations. Geoscientific Model Dev. 13, 3709–3729. https://doi.org/10.5194/gmd-13-3709-2020.

Manning, J.P., McGillicuddy, D.J., Pettigrew, N.R., Churchill, J.H., Incze, L.S., 2009. Drifter observations of the gulf of Maine Coastal current. Continental Shelf Res. 29 (7), 835–845. https://doi.org/10.1016/j.csr.2008.12.008.

Manning, J., Pelletier, E., 2014. Environmental monitors on lobster traps (eMOLT): long-term observations of New England's bottom-water temperatures. J. Operat. Oceanogr. 2 (1), 25–33. https://doi.org/10.1080/1755876X.2009.11020106.

Manning, J., Pelletier, E., 2020. Bottom water temperature collected in real-time from commercial fishing gear in gulf of Maine and southern new England shelf. SEANOE. https://doi.org/10.17882/75397.
Mannino, A., Signorini, S.R., Novak, M.G., Wilkin, J., Friedrichs, M.A., Najjar, R.G., 2016. Dissolved organic carbon fluxes in the Middle Atlantic Bight: an integrated approach based on satellite data and ocean model products. J. Geophys. Res.: Biogeosci. 121 (2), 312–336.
Marchesiello, P., McWilliams, J., Shchepetkin, A., 2001. Open boundary conditions for long-term integration of regional oceanic models. Ocean Model. 3, 1–20. https://doi.org/10.1016/S1463-5003(00)00013-5.
Mattern, J.P., Edwards, C.A., Moore, A.M., 2018. Improving variational data assimilation through background and observation error adjustments. Monthly Weather Rev. 146 (2), 485–501.
McClatchie, S., Duffy-Anderson, J., Field, J., Goericke, R., Griffith, D., Hanisko, D., Hare, J., Lyczkowski-Shultz, J., Peterson, W., Watson, W., Weber, E., Zapfe, G., 2014. Long time series in US fisheries oceanography. Oceanography. 27 (4), 48–67.
Meissner, T., Wentz, F.J., Manaster, A., Lindsley, R., 2019. Remote sensing systems SMAP ocean surface salinities [Level 3 Monthly], Version 4.0 validated release. Remote Sensing Systems, Santa Rosa, CA, USA. Available online at www.remss.com/missions/smap, doi: 10.5067/SMP40-3SMCS.
Mesinger, F., DiMego, G., Kalnay, E., Mitchell, K., Shafran, P.C., Ebisuzaki, W., Jović, D., Woollen, J., Rogers, E., Berbery, E.H., Ek, M.B., Fan, Y., Grumbine, R., Higgins, W., Li, H., Lin, Y., Manikin, G., Parrish, D., Shi, W., 2006. North American regional reanalysis. Bull. Am. Meteorol. Soc. 87, 343–360. https://doi.org/10.1175/BAMS-87-3-343.
Metzger, E.J., Helber, R.W., Hogan, P.J., Posey, P.G., Thoppil, P.G., Townsend, T.L., Wallcraft, A.J., Smedstad, O.M., Franklin, D.S., Zamudo-Lopez, L., Phelps, M.W. (2017). Global ocean forecast system 3.1 validation test. Naval Research Lab report NRL/MR/7320-17-9722, pp. 56, Stennis Space Center, MS, United States, https://apps.dtic.mil/sti/pdfs/AD1034517.pdf.
Moore, A.M., Arango, H., Broquet, G., Edwards, C., Veneziani, M., Powell, B., Foley, D., Doyle, J., Costa, D., Robinson, P., 2011c. The Regional Ocean Modeling System (ROMS) 4-dimensional variational data assimilations systems, Part III - Observation impact and observation sensitivity in the California Current. Progr. Oceanogr. 91, 74–94.
Moore, A.M., Arango, H., Broquet, G., Powell, B., Weaver, A.T., Zavala-Garay, J., 2011a. The Regional Ocean Modeling System (ROMS) 4-dimensional variational data assimilations systems, Part I - System overview and formulation. Progr. Oceanogr. 91, 34–49.
Moore, A.M., Arango, H., Broquet, G., Edwards, C., Veneziani, M., Powell, B., Foley, D., Doyle, J., Costa, D., Robinson, P., 2011b. The Regional Ocean Modeling System (ROMS) 4-dimensional variational data assimilations systems, Part II – Performance and application to the California Current System. Progr. Oceanogr. 91, 50–73.
Moore, M.I., Wilkin, J.L., 1998. Variability in the South Pacific Deep Western Boundary Current from current meter observations and a high-resolution global model. J. Geophys. Res. 103 (C3), 5439–5457.
Mulet, S., Rio, M.-H., Etienne, H., Artana, C., Cancet, M., Dibarboure, G., Feng, H., Husson, R., Picot, N., Provost, C., Strub, P.T., 2021. The new CNES-CLS18 global mean dynamic topography. Ocean Sci. 17, 789–808. https://doi.org/10.5194/os-17-789-2021.
Munroe, D.M., Narváez, D.A., Hennen, D., Jacobson, L., Mann, R., Hofmann, E.E., Powell, E.N., Klinck, J.M., 2016. Fishing and bottom water temperature as drivers of change in maximum shell length in Atlantic surfclams (Spisula solidissima). Estuar. Coast. Shelf Sci. 170, 112–122.
Neveu, E., Moore, A.M., Edwards, C.A., Fiechter, J., Drake, P., Crawford, W.J., Jacox, M. G., Nuss, E., 2016. An historical analysis of the California Current circulation using ROMS 4D-Var: System configuration and diagnostics. Ocean Model. 99, 133–151.
Powell, B.S., Arango, H.G., Moore, A.M., Di Lorenzo, E., Milliff, R.F., Foley, D., 2008. 4DVAR data assimilation in the intra-Americas sea with the Regional Ocean Modeling System (ROMS). Ocean Model. 23 (3–4), 130–145.
Rao, S. (2008). The Professional Barista's Handbook: An Expert Guide to Preparing Espresso, Coffee, and Tea, pp. 99, ISBN-10: 1-60530-098-5.
Ray, R.D., 2013. Precise comparisons of bottom-pressure and altimetric ocean tides. J. Geophys. Res. Oceans 118 (9), 4570–4584.
Remote Sensing Systems. (2017). MWIR optimum interpolated SST data set. Ver. 3.0. PO. DAAC, CA, USA. Dataset accessed 2014-06-03 at doi:10.5067/GHMWI-4FR05.
Rio, M.-H., Mulet, S., Picot, N., 2014. Beyond GOCE for the ocean circulation estimate: synergetic use of altimetry, gravimetry, and in situ data provides new insight into geostrophic and Ekman currents. Geophys. Res. Lett. 41, 8918–8925. https://doi.org/10.1002/2014GL061773.
Roarty, H., Glenn, S., Kohut, J., Gong, D., Handel, E., Rivera, E., Garner, T., Atkinson, L., Brown, W., Jakubiak, C., Muglia, M., Haines, S., Seim, H., 2010. Operation and application of a regional high frequency radar network in the Mid Atlantic Bight. Mar. Technol. Soc. J. 44 (6), 133–145.
Rogers, E., DiMego, G., Black, T., Ek, M., Ferrier, B., Gayno, G., Janjic, Z., Lin, Y., Pyle, M., Wong, V., Wu, W., Carley, J., 2009. The NCEP North American mesoscale modeling system: recent changes and future plans, in: 23rd Conference on Weather Analysis and Forecasting, Boston, Massachusetts. Available at https://ams.confex.com/ams/23WAF19NWP/techprogram/paper_154114.htm.
Seidov, D., Mishonov, A., Parsons, R., 2021. Recent warming and decadal variability of Gulf of Maine and Slope Water. Limnol. Oceanogr. 66 (9), 3472–3488.
Seroka, G., Miles, T., Xu, Y.i., Kohut, J., Schofield, O., Glenn, S., 2017. Rapid shelf-wide cooling response of a stratified coastal ocean to hurricanes. J. Geophys. Res. 122 (6), 4845–4867.
Shchepetkin, A.F., McWilliams, J.C., 2009. Computational kernel algorithms for fine-scale, multiprocess, longtime oceanic simulations. Handbook of numerical analysis. Computat. Methods Atmos. Oceans. 14, 121–183.
Sikirić, M.D., Janeković, I., Kuzmić, M., 2009. A new approach to bathymetry smoothing in sigma-coordinate ocean models. Ocean Model. 29 (2), 128–136.
Smith, P.C., Pettigrew, N.R., Yeats, P., Townsend, D.W., Han, G.Q., 2012. Regime Shift in the Gulf of Maine. Am. Fish. Soc. Symp. 79, 185–203.
Toole, J., Curry, R.G., Joyce, T., McCartney, M., Pena-Molino, B., 2011. Transport of the North Atlantic Deep Western Boundary Current about 35 N, 70W: 2004-2008. Deep Sea Research II. 58, 1768–1780.
Townsend, D.W., Thomas, A.C., Mayer, L.M., Thomas, M.A., Quinlan, J.A., 2006. Oceanography of the Northwest Atlantic Continental Shelf (1, W). In: Robinson, A. R., Brink, K.H. (Eds.), The Sea. Harvard University Press, Cambridge, pp. 119–168.
Wang, Z., 2017. NOAA National Centers for Environmental Information. Quality-controlled sea surface marine physical, meteorological and other in situ measurements from the NCEI Surface Underway Marine Database (NCEI-SUMD), https://www.ncei.noaa.gov/archive/accession/NCEI-SUMD, accessed March 2022.
Warner, J.C., Sherwood, C.R., Arango, H.G., Signell, R.P., 2005. Performance of four turbulence closure models implemented using a generic length scale method. Ocean Model. 8 (1-2), 81–113.
Weaver, A., Courtier, P., 2001. Correlation modelling on the sphere using a generalized diffusion equation. Q. J. R. Meteorolog. Soc. 127 (575), 1815–1846.
Wilkin, J., Levin, J., López, A., Hunter, E., Zavala-Garay, J., Arango, H., 2018. A coastal ocean forecast system for the U.S. Mid-Atlantic Bight and Gulf of Maine. In New Frontiers in Operational Oceanography, Proceedings of the GODAE OceanView International School 2017, E. Chassignet, A. Pascual, J. Tintore and J. Verron (Eds.), Springer, New York, 2018, 593-623.
Wilkin, J., Fleming, N., 2017. A monthly climatological analysis of the temperature and salinity of the Mid-Atlantic Bight and Gulf of Maine continental shelf, and adjacent deep ocean, by 4-dimensional weighted least squares. SEANOE. https://doi.org/10.17882/89502.
Wilkin, J., Hunter, E., 2013. An assessment of the skill of real-time models of Mid-Atlantic Bight continental shelf circulation. J. Geophys. Res. 118, 2919–2933. https://doi.org/10.1002/jgrc.20223.
Wilkin, J., Levin, J., 2022. Outputs from a Regional Ocean Modeling System (ROMS) data assimilative reanalysis (version DopAnV3R3-ini2007) of ocean circulation in the Mid-Atlantic Bight and Gulf of Maine for 2007–2021. SEANOE. https://doi.org/10.17882/89673.
Xu, Y., Cahill, B., Wilkin, J., Schofield, O., 2013. Role of wind in regulating phytoplankton blooms on the Mid-Atlantic Bight. Cont. Shelf Res. 63, S26–S35. https://doi.org/10.1016/j.csr.2012.09.011.
Zavala-Garay, J., Wilkin, J., Levin, J., 2014. Data assimilation in coastal oceanography: IS4DVAR in the Regional Ocean Modeling System (ROMS) In: Blayo, E., Bocquet, M., Cosme, E., Cugliandolo, L. (Eds.), Advanced Data Assimilation for Geosciences: Lecture Notes of the Les Houches School of Physics: Special issue June 2012. Oxford University Press, Oxford, pp. 555-576.
Zhang, W.G., Wilkin, J.L., Levin, J.C., Arango, H.G., 2009. An adjoint sensitivity study of buoyancy- and wind-driven circulation on the New Jersey Inner Shelf. J. Phys. Oceanogr. 39 (7), 1652–1668. https://doi.org/10.1175/2009JPO4050.1.
Zhang, W.G., Gawarkiewicz, G., McGillicuddy, D., Wilkin, J., 2011. Climatological mean circulation at the New England shelf break. J. Phys. Oceanogr. 41, 1874–1893. https://doi.org/10.1175/2011JPO4604.1.
Zhang, W., Gawarkiewicz, G., 2015. Dynamics of the direct intrusion of Gulf Stream ring water onto the Mid-Atlantic Bight shelf. Geophys. Res. Lett. 42, 7687–7695. https://doi.org/10.1002/2015GL065530.